The Hebrew University of Jerusalem

The Department of Applied Physics

Advanced Imaging Laboratory

Computer-Aided Surgery and Medical Image Processing Laboratory

Non-Invasive Blood Pressure Measurement using Image Processing & IR Camera

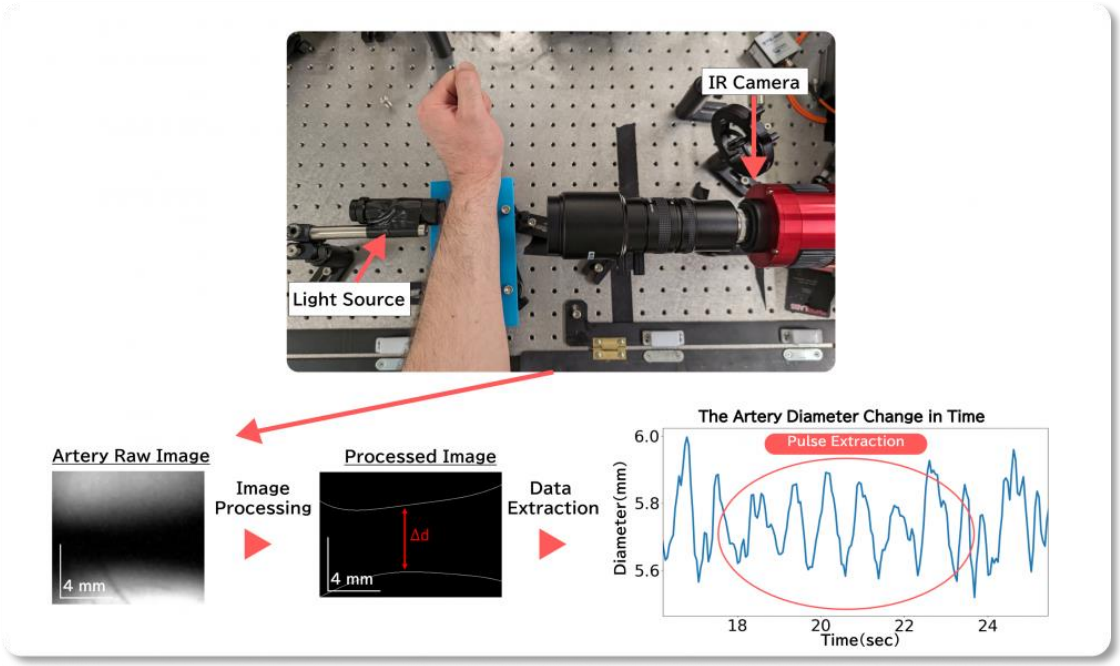

Project Members

Amit Halbreich	208917393	amit.halbreich@mail.huji.ac.il
Michael Dik	207628983	michael.dik@mail.huji.ac.il

Supervisors and Collaborators

Prof. Ori Katz | Advanced Imaging Lab - The Department of Applied Physics

Prof. Leo Joskowicz | CASMIP Lab - School of Computer Science and Engineering

Date of Submission: 30/11/2024

Table of Contents

List of Abbreviations and Symbols

- BP: Blood Pressure
- IR: Infrared
- RA: Radial Artery
- ROI: Region of Interest
- CASMIP: The Computer-Aided Surgery and Medical Image Processing Laboratory
- nm: Nanometer
- mmHg: Millimeters of Mercury
- LPF: Low Pass Filter
- FFT: Fast Fourier Transform

Abstract

Hypertension affects about one-third of adults globally, posing significant health risks such as heart disease and stroke. Despite its prevalence, nearly half of those affected are unaware of their condition, emphasizing the need for improved monitoring solutions. Our project aims to develop a non-invasive method for measuring blood pressure that can be seamlessly integrated into smartwatches.

This approach enhances awareness and management of hypertension, ultimately improving public health outcomes. The core innovation involves using image processing and infrared (IR) camera technology to measure blood pressure without physical contact. Traditional methods are often cumbersome and invasive. In contrast, our method detects subtle changes in the radial artery's volume, situated within the IR penetration depth, to provide accurate BP readings. The device differentiates arteries from veins, quantifies minute arterial changes, and calculates blood pressure using established formulas.

Our approach involves illuminating the back of the wrist with infrared light and recording a video that captures the radial artery. Advanced image processing techniques identify and quantify changes in the artery's volume over time. Currently, we are focusing on extracting the change in the artery's diameter.

Using mathematical equations, we can calculate blood pressure from these changes. The use of IR technology ensures a completely non-invasive, comfortable, and user-friendly experience. This project offers significant potential by providing an innovative, accessible method for daily blood pressure monitoring, particularly benefiting remote or underserved areas with limited access to traditional healthcare facilities.

Integrating our research into smartwatches will make it easier for users to monitor their blood pressure consistently and conveniently, leading to early detection and better management of hypertension.

Introduction

Background

Hypertension, or high blood pressure, affects approximately 1.13 billion people globally. It is often referred to as a "silent killer" because nearly half of those affected are unaware of their condition. Untreated hypertension can lead to serious health problems, including strokes, heart failure, and kidney damage. Early detection and continuous monitoring are crucial in managing this condition. Existing methods of blood pressure monitoring, such as cuff-based devices, are not suitable for continuous, real-time use, which is why developing alternative non-invasive techniques is essential.

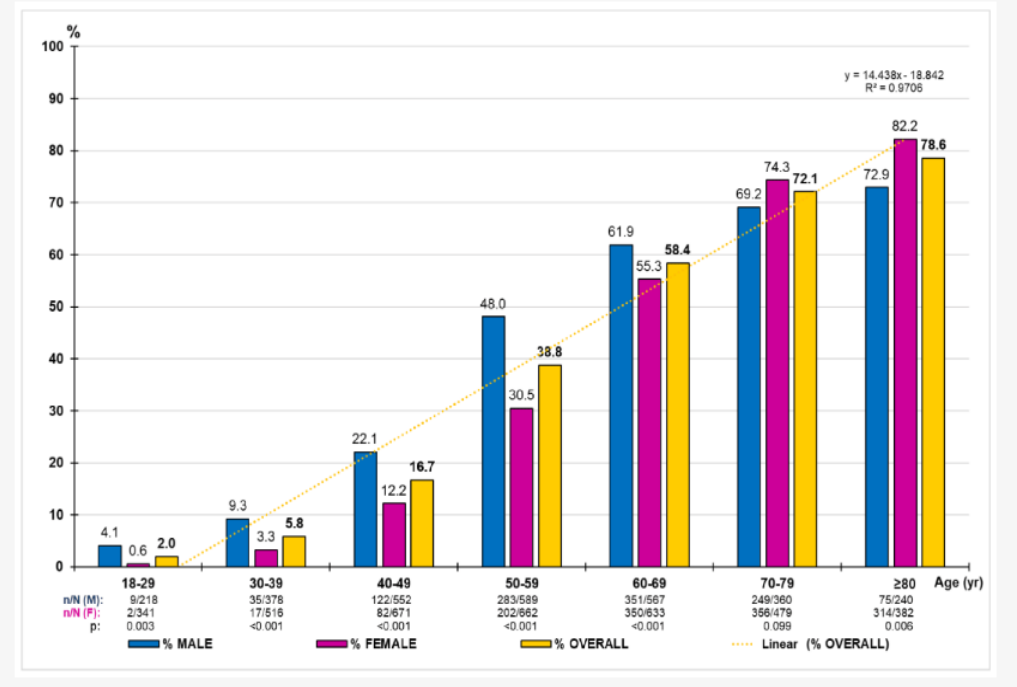

Figure 1: source [2] – *Prevalence rates of hypertension by age group according to 140/90 criterion. n: number of cases; N: sample size; M: male; F: female; p: p-value of the difference in percentages*

Objectives

The objective of this project is to design a system that uses image processing and infrared light to non-invasively detect arterial changes and calculate blood pressure in real time. By detecting changes in the diameter of the radial artery, we aim to provide accurate, non-invasive blood pressure measurements comparable to standard clinical methods.

The objective of this project is to develop a blood pressure monitoring system that is highly accessible, user-friendly, and capable of providing real-time measurements. By utilizing advanced non-invasive techniques and real-time data acquisition, the system aims to empower the general public with the ability to monitor their blood pressure autonomously. This technology seeks to provide accurate, continuous health data, thereby improving public health management and facilitating early detection and prevention of hypertension-related complications.

Scope

This project covers the use of an IR camera and image processing techniques to monitor arterial volume changes. It includes hardware design, applying image processing algorithms, testing on phantom models, and comparison with actual blood pressure readings from a BP cuff (sphygmomanometer) and compare pulse extraction from our solution with smartwatch and BP cuff traditional heart-rate readings.

Organization

The project book is structured as follows: A literature review will provide an overview of the state-of-the-art technologies for blood pressure measurement. The

methodology section will describe the design and implementation of the system including explanations on different conducted experiments. Finally, testing results will be presented and discussed, followed by conclusions and suggestions for future work regarding enhancing our solution and image processing algorithm.

Literature and State-of-the-Art Review

Continuous monitoring of blood pressure (BP) is crucial for managing cardiovascular diseases, yet traditional cuff-based methods are inconvenient for continuous use. Recent advancements have focused on developing wearable, non-invasive devices that provide continuous BP monitoring without the need for a cuff.

Ultrasound-Based Methods

Wang et al. (2021) developed a wearable ultrasonic device capable of continuous BP monitoring by capturing central blood pressure waveforms [source 1]. The device uses ultrasonic transducers to detect arterial wall movements, allowing for the estimation of BP based on the arterial diameter and its pulsatile changes. This method offers high accuracy and the potential for real-time monitoring.

Similarly, wearable ultrasound patch technologies have been explored to provide continuous, non-invasive BP measurements by assessing the mechanical properties of arterial walls [source 1]. These methods leverage the ability of ultrasound to penetrate tissue and provide detailed images of arterial structures.

Limitations

Despite their advantages, ultrasound-based methods face limitations such as device complexity, cost, and the need for precise placement to obtain accurate measurements. Moreover, the penetration depth of ultrasound may be insufficient for certain applications, and the technology may not be easily accessible for widespread use.

Infrared Light for Blood Pressure Measurement

We chose to use infrared (IR) light for our project because it penetrates deeper into skin tissue than visible light, allowing for effective transillumination of the hand to visualize underlying blood vessels. Unlike ultrasound, which can be limited by device complexity, cost, and the need for precise placement, IR light provides a simpler and more accessible method for detecting arteries and veins. By shining IR light through one side of the hand and capturing a video from the opposite side, we can identify blood vessels as they absorb more IR light and appear darker in the images. This enables us to monitor changes in arterial volume over time, allowing for non-invasive blood pressure measurement similar to ultrasound-based techniques but with fewer limitations.

Theoretical Background

Blood pressure is typically measured as the force exerted by circulating blood on the walls of arteries. This project leverages changes in arterial volume as a proxy for blood pressure, based on the principle that arterial diameter fluctuates with each heartbeat. By focusing on the radial artery, which is close to the skin surface and detectable using infrared light, we can monitor these changes non-invasively. The IR spectrum allows us to penetrate deeper layers of tissue, capturing images that reveal subtle arterial shifts during the cardiac cycle. Traditional BP measurements rely on cumbersome devices that require periodic manual monitoring, limiting accessibility and real-time insights. This project seeks to address these limitations through a non-invasive approach, leveraging changes in arterial volume and advanced imaging techniques.

Blood pressure is a critical physiological parameter, traditionally measured as the force exerted by circulating blood on arterial walls. Accurate and continuous monitoring of blood pressure is essential for diagnosing and managing cardiovascular diseases, particularly hypertension, which poses a significant health risk worldwide. This project aims to develop a non-invasive method for blood pressure monitoring by analyzing arterial volume changes using infrared (IR) light and image processing techniques.

The arterial system, specifically the radial artery, located just beneath the skin at the wrist, provides a suitable site for such measurements. As illustrated in the source [5] image, the penetration of light into biological tissues varies with wavelength. Infrared light, with its superior penetration capabilities, enables us to reach deeper layers of the skin, including the arterial walls, while minimizing scattering. By illuminating the radial artery and capturing video frames through an IR camera, we can track subtle changes in arterial diameter, which are directly correlated with the cardiac cycle.

The source [4] image highlights the importance of blood pressure dynamics, where systolic pressure corresponds to the contraction phase of the heart and diastolic pressure to its relaxation. These phases result in measurable variations in arterial volume, which are key to the proposed imaging technique. Using advanced algorithms, these volumetric changes are extracted from the recorded frames using sophisticated Image Processing algorithm to provide a continuous representation of the cardiac cycle and blood pressure.

Lastly, the source [3] image demonstrates the anatomical structure of the radial artery and its accessibility for imaging using IR light. By simulating tissue layers with biological materials, such as chicken breast, and incorporating a silicone tube to replicate arterial pulsations, this project validates the feasibility of the method. The experimental setup ensures that the algorithm can detect arterial changes through scattering media, paving the way for real-world applications conducted on human subjects in wearable devices like smartwatches for continuous blood pressure monitoring.

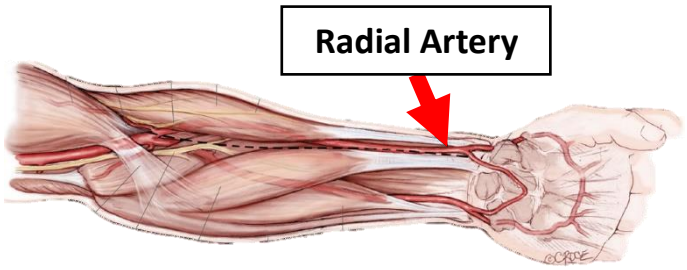

Figure 2: source [3] – *Radial Artery location in wrist.*

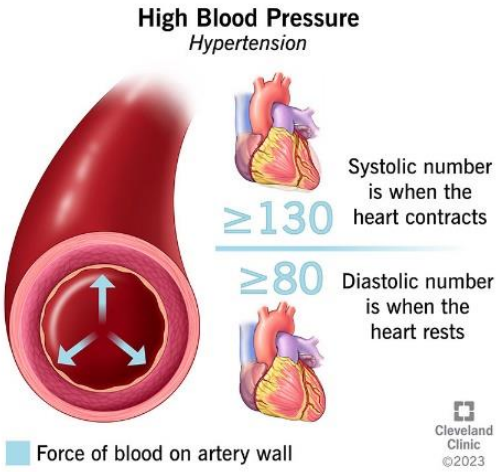

Figure 3: source [4] – *Arterial Walls Chamges corresponding to BP changes.*

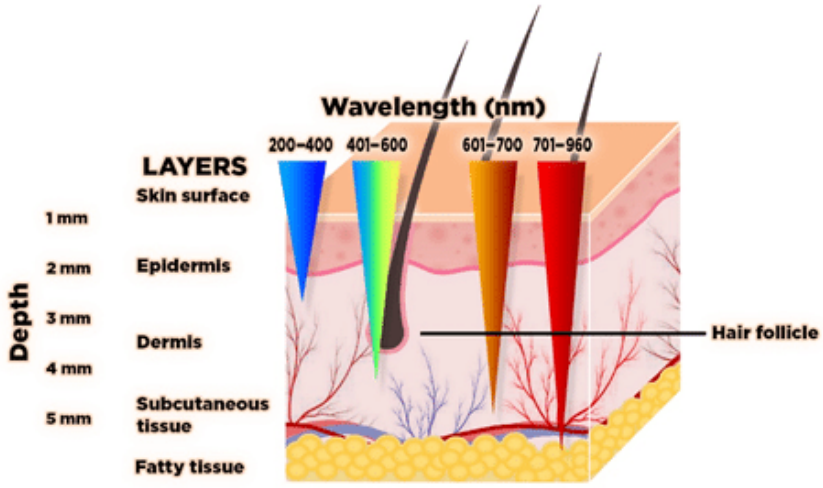

Figure 5: source [5] – *Skin tissues penetration at different wavelength.*

Methodology and Implementation

1. Phantom Experiment - Ground Truth Experiment

Design and Development

The goal of this experiment was to simulate arterial behavior under controlled conditions, providing ground truth data to validate the system's accuracy. A silicone tube mimicked the radial artery, and chicken breast layers simulated human skin tissue. A servo motor applied pulsatile movements to the silicone tube, replicating arterial contraction and dilation.

Method

We conducted a ground truth experiment to demonstrate that we can measure changes in the artery and to validate that the data we will extract from human skin is accurate.

To imitate the artery, we chose a silicone tube with a diameter of 2mm (the actual artery diameter is 2.3mm) and applied a thin layer of red color to it. We tried different methods of coloring, but in other methods, the color was peeling off. Additionally, we wanted to maintain the 2mm diameter, and spraying the tube provided us the best results.

1) *2)* *3)*

Figure 6: *Different silicone tube coloring*
1) Left: No Coloring, **Middle:** Acrylic Coloring **Right:** Sprayed Silicone Tube

We simulated the arterial changes by connecting one end of the tube to a fixed point and the other end to a servo motor that we could control. The servo rotated between 35-165° degrees with a delay of one second on each side, which provided us with the data shown in one of the pictures (stretched vs. not stretched).

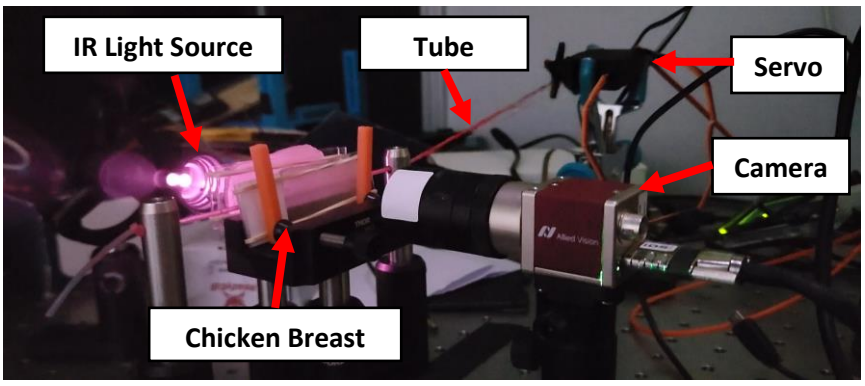

Figure 7: *Phantom experiment setup*
The system includes: IR Light Source, 2 Chicken Breast pieces, a silicone tube, Servo Motor & IR Camera

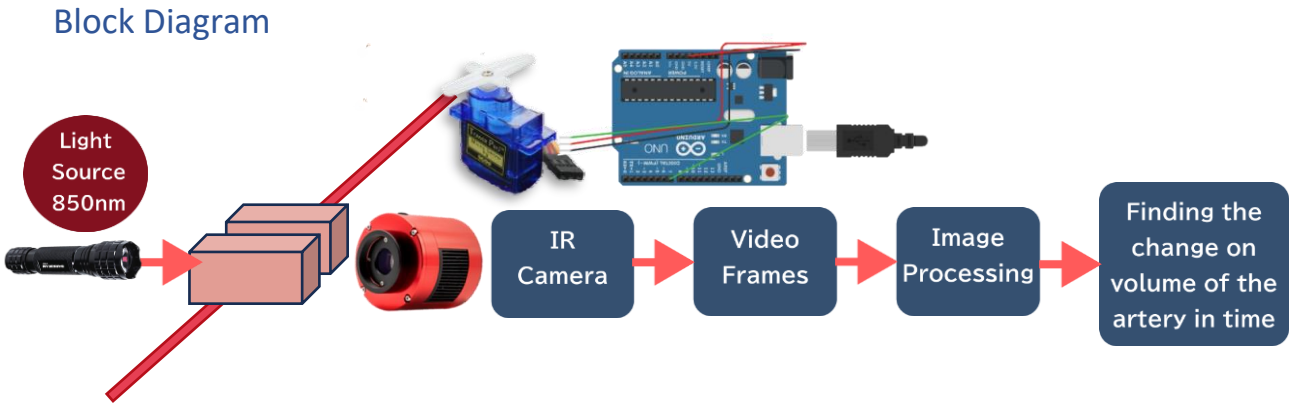

Figure 8: *Ground Truth Experiment - Algorithm Process - Block Diagram*

Challenges and Solutions

- Light Scattering: Chicken breast layers introduced scattering, making boundary detection challenging. The solution was to limit thickness to ≤2.5mm and refine thresholding algorithms.

Tube Coloring: Initial coloring methods peeled off; spraying the tube provided uniform absorption and maintained diameter integrity.

Tools and Equipment

- ZWO ASI990MM-PRO IR camera with SenSWIR IMX990 sensor for capturing images across wavelengths ranging from 400nm to 1700nm.
- Silicone tube (2mm diameter) to replicate the artery.
- Arduino Uno SMD R3 with ATmega328P MCU + USB Connector.
- Servo motor to generate pulsatile movements.
- IR camera (ZWO ASI990MM-PRO) for capturing the arterial motion.
- Chicken breast tissue layers to mimic skin scattering and absorption.
- Python-based software for video processing and data analysis.

The system's design revolves around an infrared camera, specifically the ZWO ASI990MM-PRO, to capture real-time images of the radial artery. This camera is selected for its advanced sensitivity in the short-wavelength infrared (SWIR) range, enabled by Sony's IMX990 sensor based on SenSWIR technology. The ASI990MM-PRO offers a broad spectral response from 400nm to 1700nm, allowing for deeper tissue penetration and clearer visualization of arterial structures beneath the skin surface.

Figure 9: *[source 8]ZWO ASI990MM-PRO Camera.*

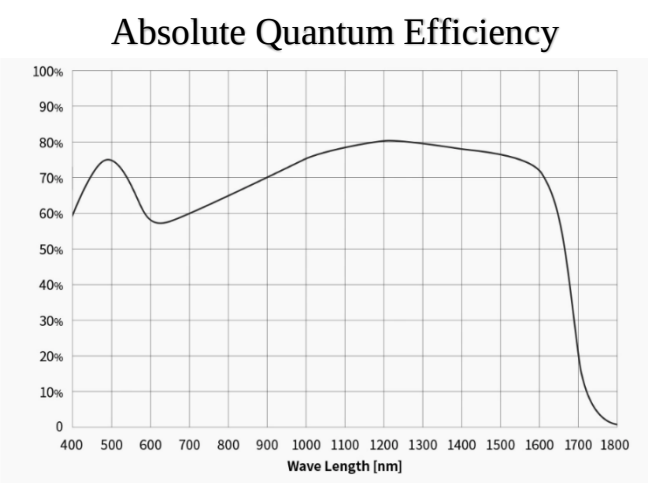

Figure 10*: [source 8] – ZWO ASI990MM-PRO Absolute Quantum Efficiency Plot.*

Procedures

1. Set up the silicone tube with one end fixed and the other connected to a servo motor.
2. Place chicken breast layers of varying thickness (1–4 mm) between the IR camera and the tube.
3. Illuminate the tube using IR LEDs and capture video recordings.
4. Process the video frames to extract arterial diameter changes using binary thresholding and blurring algorithms.

Hardware Implementation

- The silicone tube was painted red to enhance IR light absorption.
- The servo motor was programmed to apply a 1-second delay.
- IR LEDs provided uniform illumination, ensuring clear imaging of the tube through chicken breast layers.

Software Implementation

- Extracted frames from video recordings.
- Applied 3 different methods to detect tube boundaries.

We primarily use three different algorithms to detect the artery, and we evaluate each of them against the ground truth to decide which algorithm to proceed with.

1. **Binary algorithm with a fixed threshold**: We manually tuned the threshold to achieve optimal results.
2. **Otsu's adaptive threshold algorithm**: An adaptive method that automatically finds the optimal threshold.
3. **A custom algorithm based on image gradient**: We developed this to detect edges by analyzing the gradient changes in pixel intensity.

1)

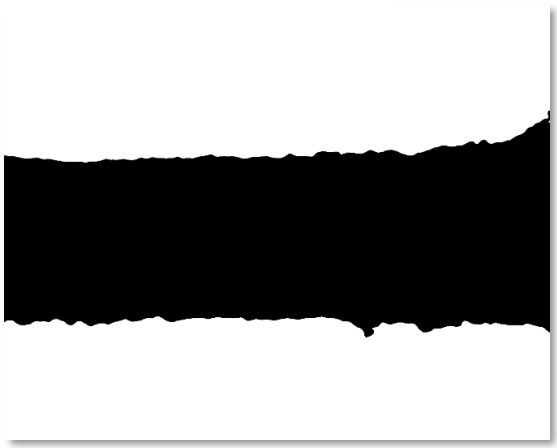

2)

3)

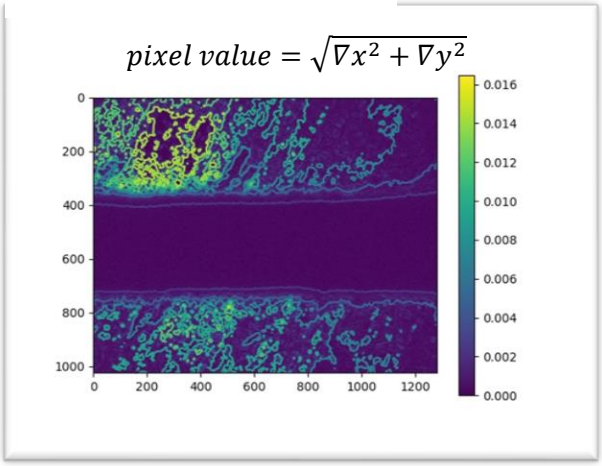

4)

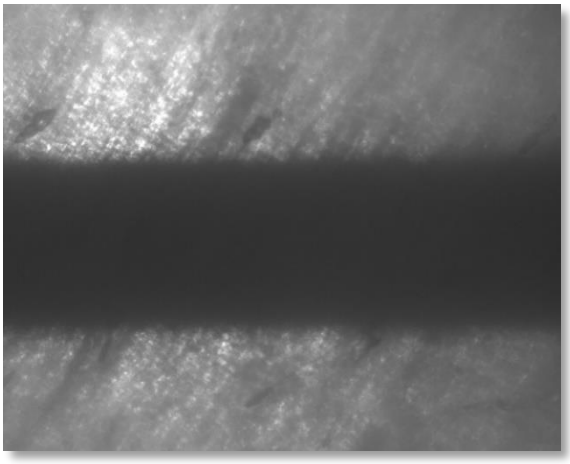

Figure 11: *Different algorithm results*
1) Top-Left: Binary Threshold, **2) Top-Right:** Otsu's Adaptive Threshold
3) Bottom-Left: Image Gradient, **4) Bottom-Right:** Raw Image

Using the custom gradient algorithm, we can accurately identify changes in the artery's area (Δ). This identification is achieved by calculating the pixel gradient as $pixel\ value = \sqrt{\nabla x^2 + \nabla y^2}$, which highlights regions of intensity variation. The inner line, corresponding to the arterial boundary, is clearly delineated due to the sharp gradients at the edges of the artery. In contrast, the outer line exhibits higher noise levels, resulting from weaker gradients and external tissue interference. This method ensures that the detection process is algorithm-driven, minimizing subjective manual input and enhancing reproducibility in the analysis.

The gradient map reveals areas of **high derivative changes**, represented by **yellow and green** regions, which correspond to **significant intensity variations**. Conversely, **blue and purple** regions denote areas with **low derivative changes**, indicating **minimal intensity variation**. Upon analysis, we observed that the custom gradient algorithm produced inconsistent artery boundaries between different frames and 2 indistinguishable inner and outer boundaries on the same frame, particularly under conditions with high noise or scattering. These inconsistencies undermined its reliability for detecting arterial edges.

To determine the effectiveness of the other 2 algorithms we measured the changes in the diameter of the tube between contraction and expansion through time and compared and analyzed the 2 graphs received from Otsu's Adaptive Threshold and Fixed Threshold algorithms:

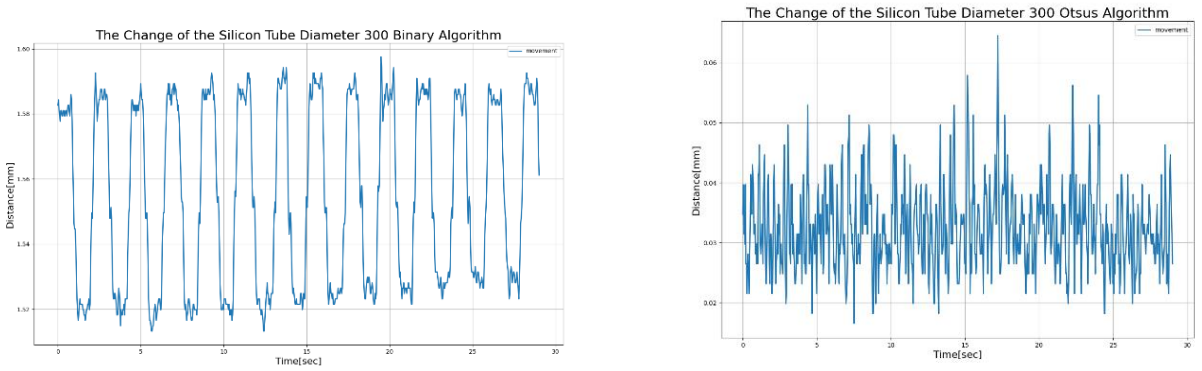

Figure 12: *Ground Truth Experiment – Binary Threshold* ***[Left]*** *VS Otsu's Adaptive Threshold* ***[Right]*** *algorithms comparison*

The results obtained using Otsu's Adaptive Threshold algorithm exhibit significant noise, making it difficult to distinguish the two distinct phases of contraction and expansion of the silicone tube. This lack of clarity indicates the algorithm's sensitivity to minor variations in pixel intensity, which amplifies noise and hinders the identification of periodic arterial changes. In contrast, the Fixed Threshold algorithm applied to the frames produces well-defined phases of contraction and expansion, accurately capturing the cyclic nature of the tube's diameter changes. After benchmarking its performance against the results from the ground truth experiment, we opted to adopt the binary thresholding algorithm. This method demonstrated greater robustness and accuracy in delineating arterial boundaries, making it a more reliable choice for our application.

Results

On this experiment we examine if the existence of a scattering medium, as a chicken breast tissue changes the overall change (Δ) in the diameter of the artery over time.

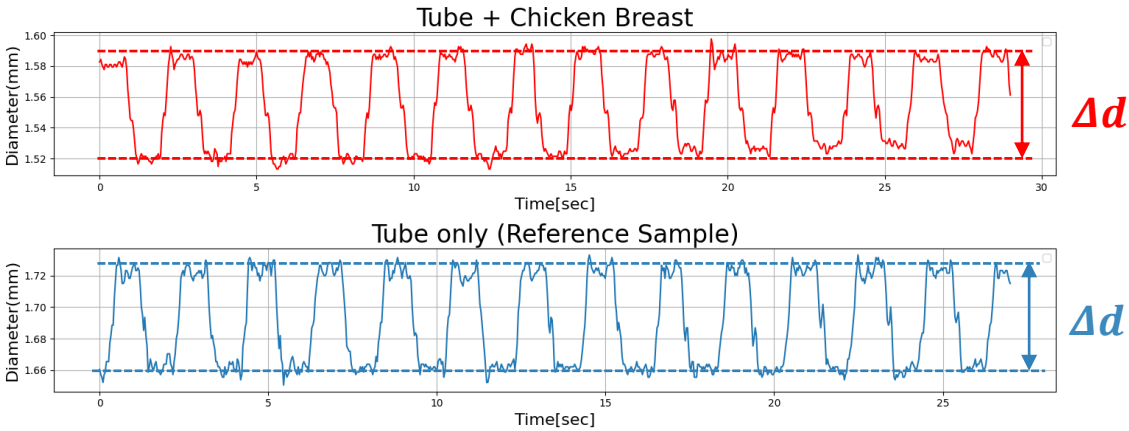

Figure 13: *Direct Imaging VS Skin Mimic Comparison*

Same change in diameter: $\boldsymbol{\Delta d = 0.7 \pm 0.03[mm] = \Delta d}$

Analysis

The results show that we obtained very similar graphs, where the red curve represents the outcome using chicken breast, which simulated a human wrist, and the blue curve corresponds to the same experiment but with a silicone tube without any scattering medium. The critical part of our measurement is the change in the artery. This similarity between the two graphs demonstrates that, despite the differences introduced by the medium, the arterial change remains consistent, marked as the red and blue deltas. These results allowed us to proceed to the next phantom experiment.

To mimic the skin tissue, we used layers of chicken breast cut into different sizes and measured their thicknesses, ranging from 1mm to 4mm. We placed these samples between lab glass slides and positioned them between the silicone tube and the camera. From our experiments, we determined which algorithm worked best for us. We showed that up to a thickness of 2.5mm, we could clearly observe the changes, and the results were close to those we achieved without the chicken breast. Although we observed a shift due to scattering, the crucial measurement of detecting the changes in the tube was correctly identified.

Figure 14: *Chicken Breast in varying thickness levels*
Left to right thickness levels: 3.6mm, 2.75mm, 2.5mm, 2.27mm, 2.0mm

2. Conducting Experiments on Various Wavelengths

Design and Development

This experiment aimed to identify the optimal IR wavelength for detecting arterial changes through scattering tissue. Various wavelengths were tested to evaluate their penetration depth, scattering, and imaging clarity.

Tools and Equipment

- ZWO ASI990MM-PRO IR camera with SenSWIR IMX990 sensor for capturing images across wavelengths ranging from 400nm to 1700nm.
- IR LEDs emitting at wavelengths of [850,940,970,1050,1450,1550] nm selected based on their penetration and absorption profiles in biological tissues[source 9] and conducted wavelength experiments to determine the optimal IR wavelength for RA imaging. The following laser diodes and LEDs were used [Appendix B]:
    - **M1550L4 (1550 nm)**.
    - **M1450L4 (1450 nm)**.
    - **M1050L4 (1050 nm)**.
    - **M970L4 (970 nm) & M940L3 (940 nm)**.
    - **850nm LED**.
    - **680nm LED**.
- Telephoto lens.
- Power and current meter for to quantify measurements.
- Black metal object with high level of IR light absorption.
- Millimetric paper with white background for maximum scattering.
- Spectral analysis software for evaluating light absorption and penetration.

Procedures

1. Select a fixed relative power level similar as possible for each wavelength – around 40-60[mW] for optimal imaging – we verified it earlier from an article.
2. Illuminate the metal object with IR light at different wavelengths on the subject's skin and on the millimetric paper.
3. Capture frames of the metal object with the camera on skin tissues.
4. Measure pixel intensity across the artery region to assess contrast and clarity.
5. Compare results across wavelengths using a combination of amplitude height, power level, and scattering reduction metrics using python software.

To effectively illuminate the region of interest (RIO) on the wrist, the design includes LEDs emitting IR light [850,940,970,1050,1450,1550] nm at a specific wavelength within the SWIR and NIR spectrum. We selected this wavelength based on the absorption and penetration characteristics of light in biological tissues determining which wavelength would work best for visualizing arterial structures [source 9]. By reviewing data from other research studies, we identified optimal wavelengths that enhance contrast between blood vessels and surrounding tissues [source 10].

We then chose the closest matching wavelength available from the Thorlabs catalog to implement in our system. The IR LEDs provide uniform illumination across the wrist area, enabling the camera to detect subtle changes in arterial volume resulting from pulsatile blood flow.
To effectively illuminate the ROI on the wrist, we selected LEDs emitting infrared light at specific wavelengths of 850 nm, 940nm, 970nm, 1050nm, 1450 nm, and 1550nm. Our choice was guided by analyzing the absorption and penetration characteristics of light in biological tissues to achieve deeper penetration and clearer visualization of arterial structures. Initially, we focused on absorption and penetration depth, intentionally overlooking the scattering and absorption of light in water.

During our experiments, we realized that light scattering in water is a crucial factor affecting image quality. When we compared the results across the selected wavelengths, we found that the best images were obtained at 850nm. This wavelength corresponds to the lowest scattering coefficient in water among the wavelengths we chose, resulting in enhanced clarity of the arterial images.

We also began conducting experiments at wavelength 680nm, although these are still in progress. Preliminary results at this shorter wavelength appear promising, suggesting that lower wavelengths may further reduce scattering and improve imaging contrast. However, more research is needed to fully understand the implications and optimize our choice of wavelengths. Future work will focus on refining these findings to enhance the system's performance in non-invasive blood pressure measurement.

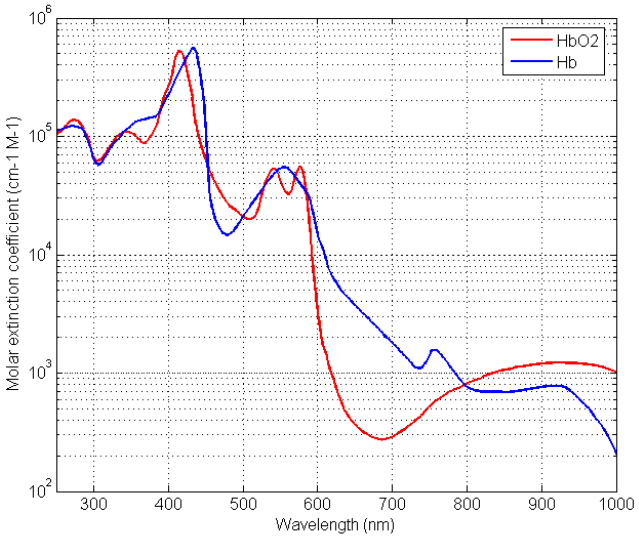

source [6] – **Figure 15:** The molar extinction coefficients of HbO2 and Hb. We can clearly see that the absorption significantly decreases from 600 nm and above.

Challenges and Solutions

- **Focus Discrepancies:** Different wavelengths required varying focal lengths. Switching to a telephoto lens resolved focus issues across all wavelengths.
- **Scattering Variability:** Preliminary tests revealed significant scattering at 1450 nm and 1550 nm; these wavelengths were deprioritized for further testing.

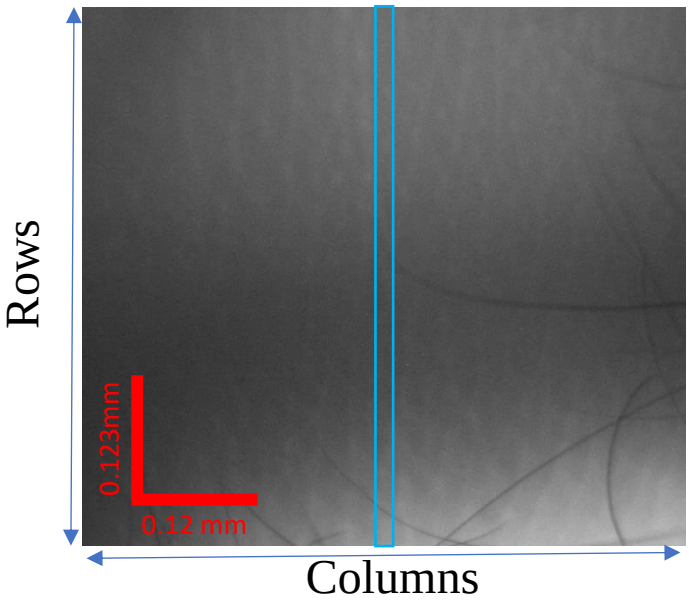

Figure 16: example of Raw Image of the RA projected with 850 nm light.
In red reference for size and the box in blue is the ROI for our calculation and graphs.

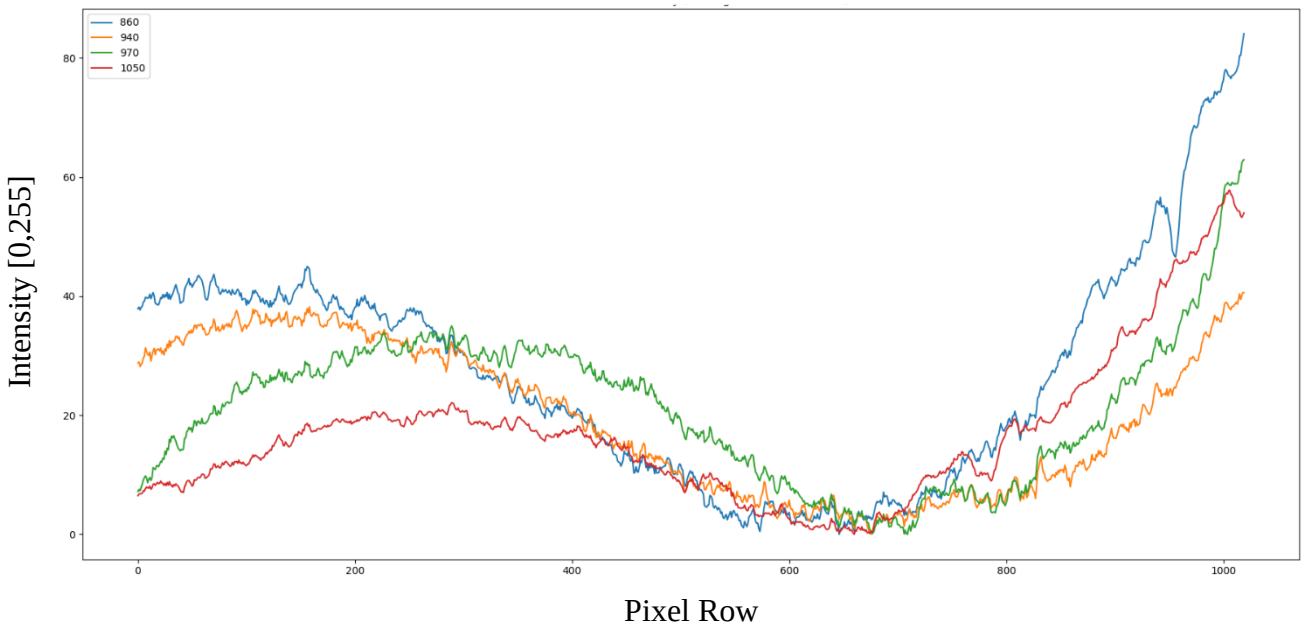

Graph 1: Observation of different wavelength in the artery (result normalized)

We already clearly see that the blue graph has the strongest change between the observed area (the absorption of light due to the artery) and compare to the tissue around it.

To obtain even more accurate results, we placed a metal object in front of the hand to observe the light passing through it. This allowed us to determine which light penetrates the hand most effectively. For this experiment, we used aluminum as the metal object. Here are the results.

Metal Object Reference

To validate the observed light penetration through human tissue, a black metallic object (aluminum) was placed in front of the light source and the hand. The metallic object served as a reference to verify the expected absorption and scattering patterns. Before each experiment, the output power of the light source was measured to ensure consistency across tests.

Test Object on Human Skin

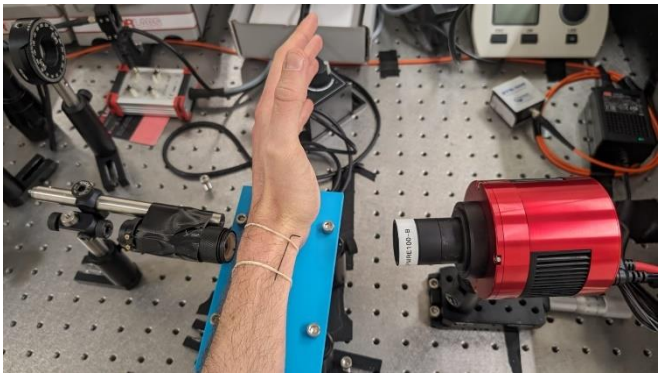

Figure 17: Lab setup for measuring different wavelength.

Metallic Object Size of 0.7mm

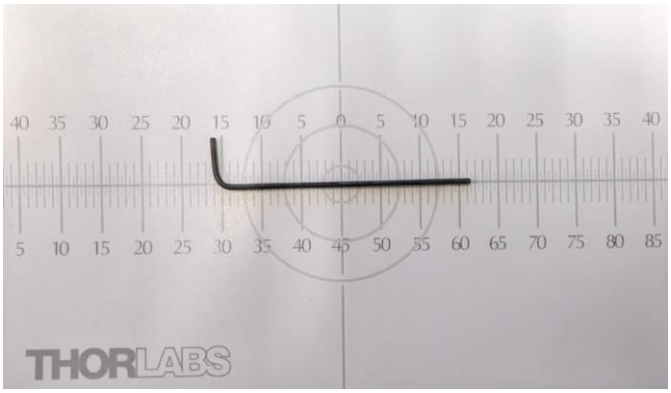

Figure 18: The metal object placed on hand.

Selection of Wavelength

The molar extinction coefficients of oxygenated and deoxygenated hemoglobin (HbO_2 and Hb) guided the wavelength selection. To compare the effectiveness of each wavelength, images of the radial artery were captured, and the grayscale intensity of pixels within the artery region was averaged. For consistency, all captured images were 1288x1024 pixels, corresponding to a physical area of 22x18 mm.

The analysis involved:

1. Selecting the artery region (highlighted in blue in the images).
2. Calculating the average grayscale [0,255] intensity for each column in the selected region.
3. Subtracting the minimum value from the intensity data to normalize the results.

4. Plotting the normalized intensity values for each wavelength to compare the arterial signal against the surrounding tissue.

<u>How we chose which wavelength to work with</u>**:**
we took an image of each wavelength we took frame of the artery seen well in the middle and we took the average of the color in gray scale [0,255]

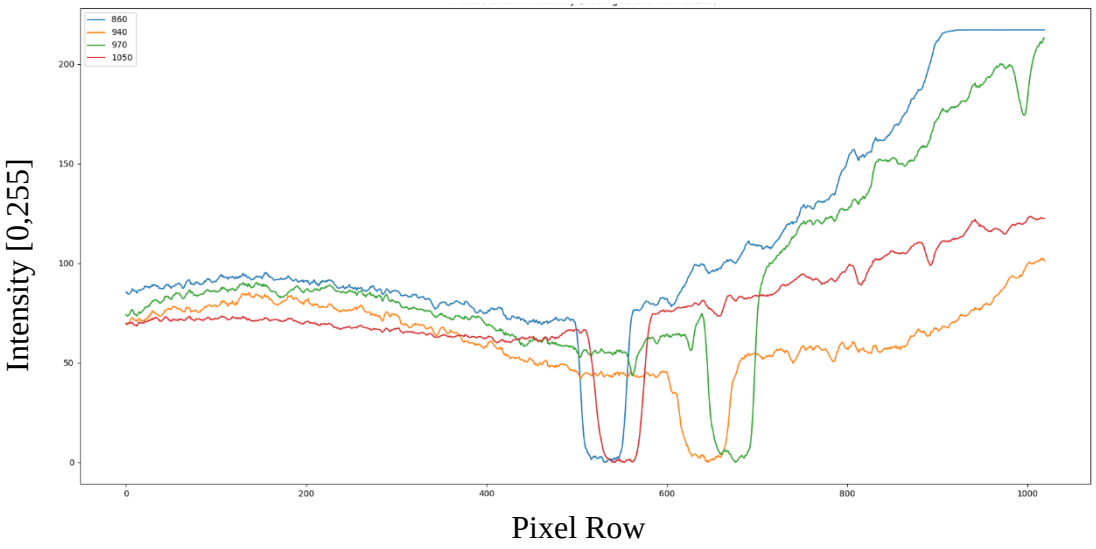

Graph 2: Observation of different wavelength in the metal object (result normalized)

Data Refinement: To normalize the data for better comparison

- Averages were calculated for a stable region ([0, 50] pixels).
- The data were adjusted to a negative scale for visualization clarity.
- A window of 100 pixels to the left and right of the minimum values was used to calculate averages and refine peak detection.

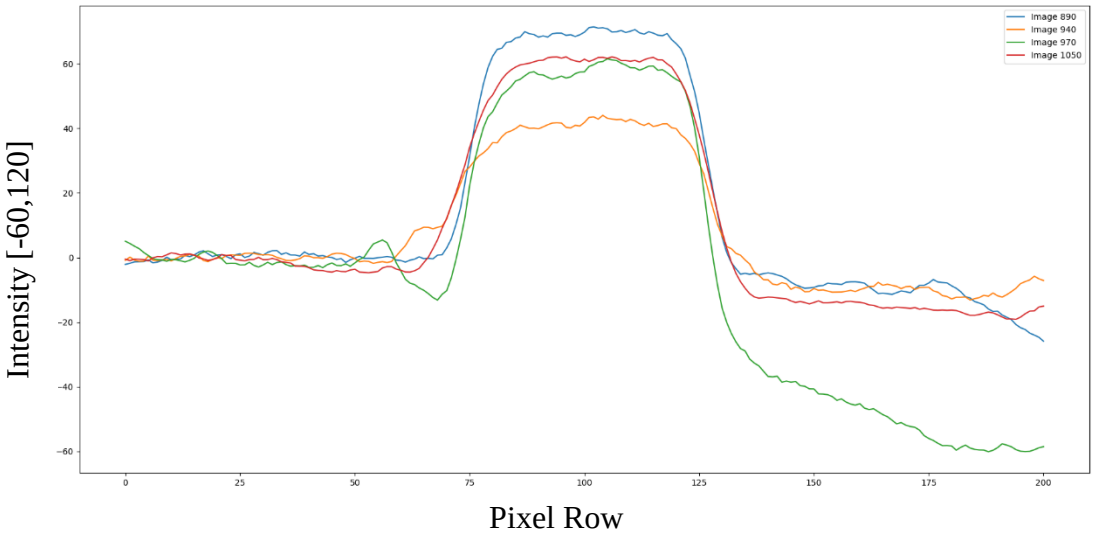

Graph 3: Observation of different wavelength in the metal object (result normalized)

Results Analysis

We quantify the efficiency of using the specific LED wavelength according to 3 parameters: Power, Amplitude Height, Width of Half-Maximum.

We selected the IR wavelength according to:

- Lower Power level.
- Higher Amplitude Height.
- Lower Width of Half-Maximum.

Lower Power Pros: allows safer work environment for experiments, allows better results and imaging using less power.

Higher Amplitude Height Pros: The arterial change is more likely to be visible to the IR Camera.

Lower Width of Half-Maximum Pros: The level of the boundaries spreading is lower which allows sharper images and better results analysis options.

We calculated the width of each peak of the Heaviside function, as we aimed for the narrowest width of half-max distribution. The results are shown in the following table:

Wavelength[nm]	Power [mW]	Amplitude Height [0,255]	Width of Half-Maximum [mm]
860	**44.5**	$\mathbf{70 \pm 1}$	0.867 ± 0.02
940	60.5	42 ± 0.7	0.918 ± 0.02
970	51.1	60 ± 1.9	$\mathbf{0.833 \pm 0.02}$
1050	47.4	63 ± 1.7	0.884 ± 0.02
1440	13	_	_
1550	5	_	_

Table 1: Results of different wavelengths parameters extracted from "Graph 3"

The results showed that the 850 nm wavelength displayed the highest amplitude height (70) with a relatively low width of half-maximum ($0.867\ mm$), indicating sharp boundaries and strong absorption by the artery. In contrast, the 970 nm wavelength, while achieving a good balance between amplitude height (60) and width of half-max ($0.833\ mm$), did not perform as well as 850 nm in terms of overall amplitude and clarity. Graphs derived from this data clearly demonstrate that 850 nm offers the best trade-off between power, amplitude, and width, making it the most suitable for imaging arterial changes with minimal noise and high clarity. Its sharp arterial edges and distinct contrast between the artery and surrounding tissue are essential for real-time blood pressure monitoring.

3. Conducting Experiments on Human Subjects

Design and Development

The project involves the development of a non-invasive system for monitoring blood pressure (BP) using IR imaging and image processing techniques. The design includes an IR light source to illuminate the wrist, specifically targeting the radial artery, and an IR camera to capture real-time images. The radial artery was selected for its superficial position and ease of visualization. The system design involves a ground-truth validation process using phantom models, followed by human trials to ensure accuracy and reliability.

Tools and Equipment

- **Hardware:**
    - ZWO ASI990MM-PRO IR camera with SenSWIR IMX990 sensor for capturing images across wavelengths ranging from 400nm to 1700nm.
    - IR LEDs emitting at wavelength of 850nm selected based on their penetration and absorption profiles in biological tissues and conducted wavelength experiments to determine the optimal IR wavelength for RA imaging.
    - Custom 3D printed comfortable arm mount.
    - BP cuff (sphygmomanometer) and smartwatch for heart-rate cross validation in comparison to our received results.
- **Software:**
    - Python-based algorithms for image processing and analysis.
    - OpenCV for image manipulation and thresholding.
    - NumPy for signal processing - Fast Fourier Transform (FFT) for extracting the heart rate from diameter changes.
    - Matplotlib for data visualization and plotting.
    - ASIStudio software for video capturing with ZWO ASI990MM-PRO IR camera.

Procedures Overview

- **Experiment Workflow**
    - Position the IR camera and light source on a stable mount, aligned with the radial artery.
    - Illuminate the participant’s wrist and record videos of the artery under different conditions.
    - Extract frames and process them to measure arterial diameter changes using binary thresholding.
    - Compare the frequency components extracted via FFT with smartwatch and conventional cuff-based BP recorded heart rate and BP data for validation.

- As a reference, we measured the heart rate using smartwatch at the beginning of the experiment

Block Diagram

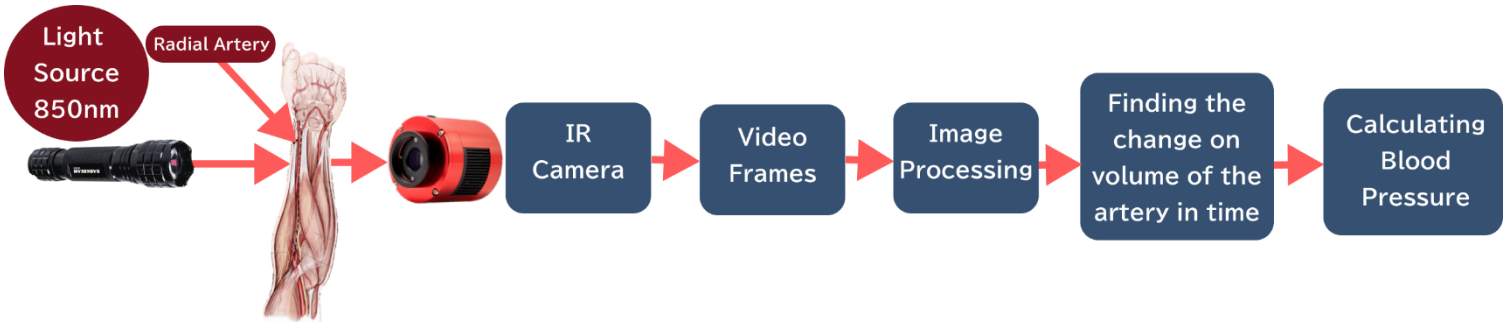

Figure 19: *Human Experiments: Algorithm Process - Block Diagram*

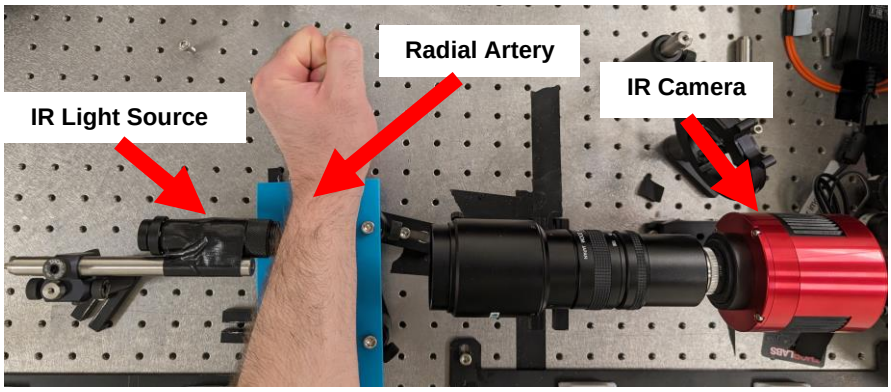

Figure 20: Human Experiments – Lab Setup

Image Processing

- Binary Thresholding: A fixed threshold value was applied to grayscale images to detect artery boundaries.
- Median Blurring: Applied a kernel of fixed size to reduce noise and enhance boundary clarity.
- Cropping: Focused on regions of interest (ROIs) using a pre-defined coordinate system for consistent analysis.

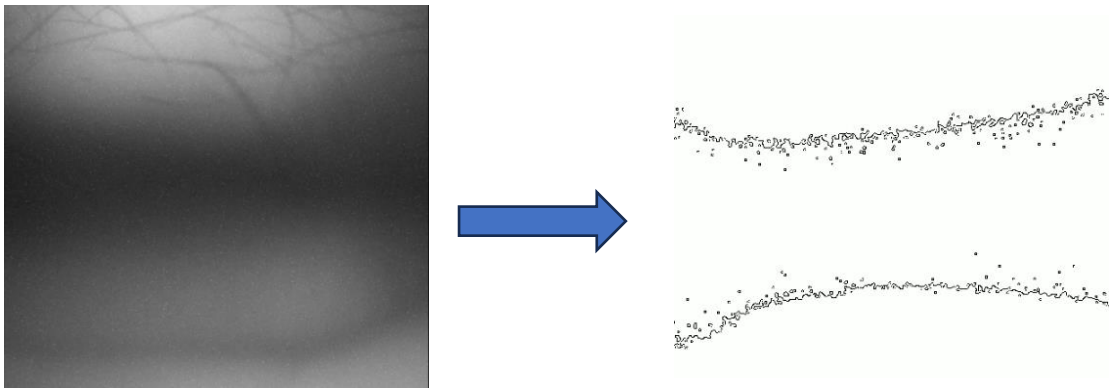

Figure 21: Left: Radial raw image, **Right:** Radial Artery after applying image processing algorithm

- Raw Data: The raw frames displayed limited contrast and significant noise, making it challenging to discern arterial movement.
- Processed Data: After applying the algorithm, the arterial diameter changes were distinctly visible, allowing the system to detect pulse-related fluctuations accurately.
- The processed video output showed periodic expansion and contraction of the artery, reflecting the cardiac cycle.

While working with human data, we made some adjustments to the existing algorithm we previously developed in the Ground Truth experiment phase, by incorporating Median Blurring:

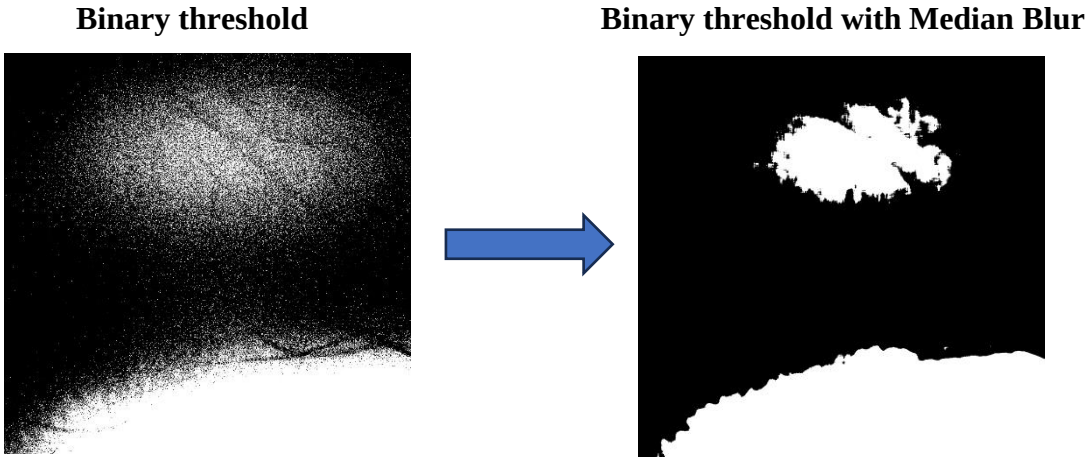

Figure 22: Algorithm changes – **Right:** Binary Threshold VS **Left:** Binary Threshold with Median Blurring Comparison

We enhanced the algorithm's performance on human data by integrating a Median Blurring filter. This effectively reduced the "salt and pepper" noise in binary threshold images, improving the clarity of detected arterial edges and ensuring more robust boundary detection even in challenging noise conditions.

- ❖ Feature Extraction:
  - Distance between arterial walls was measured for each frame using the largest sequence of connected black pixels in grayscale images.
  - Moving averages smoothed these measurements to remove high-frequency noise.
- ❖ Signal Processing:
  - Fast Fourier Transform (FFT) was applied to detect heart rate frequency components from the pulsatile diameter changes.
  - Frequencies outside the expected range 0-0.5 Hz were filtered out using LPF, and inverse FFT reconstructed the refined signal for final analysis.

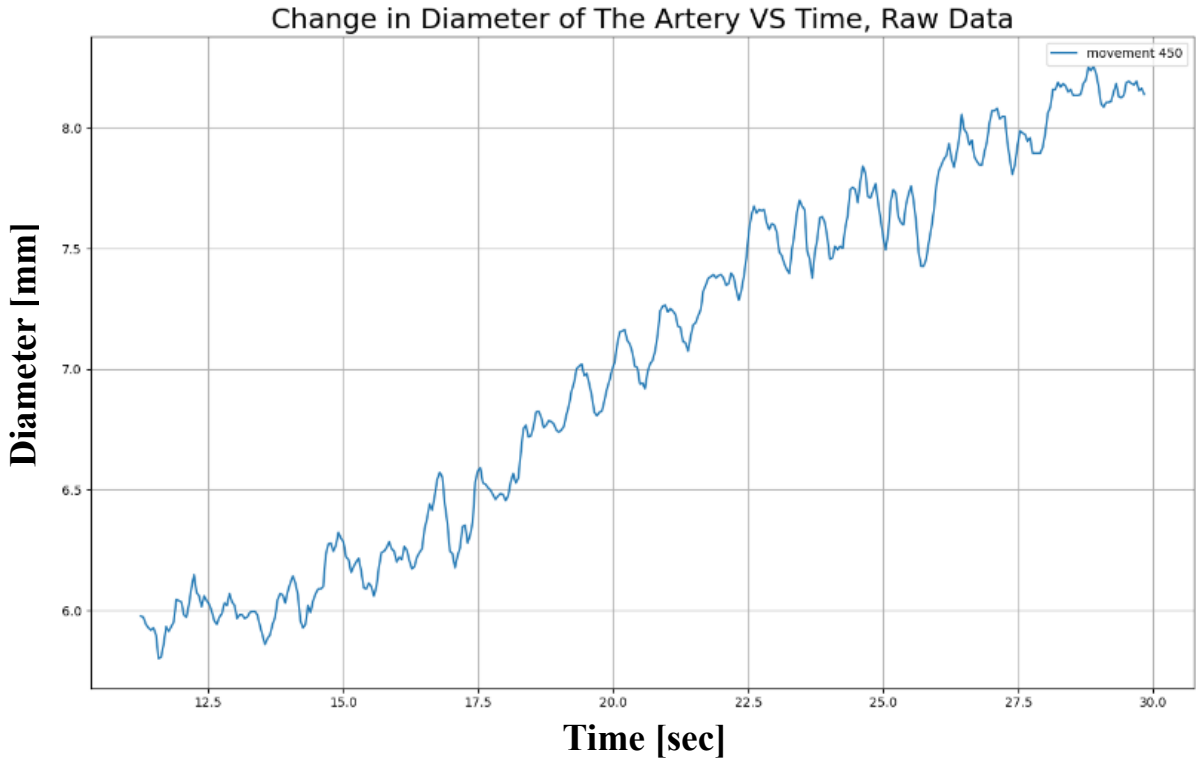

Figure 23: *Raw Data before applying moving average and LPF*

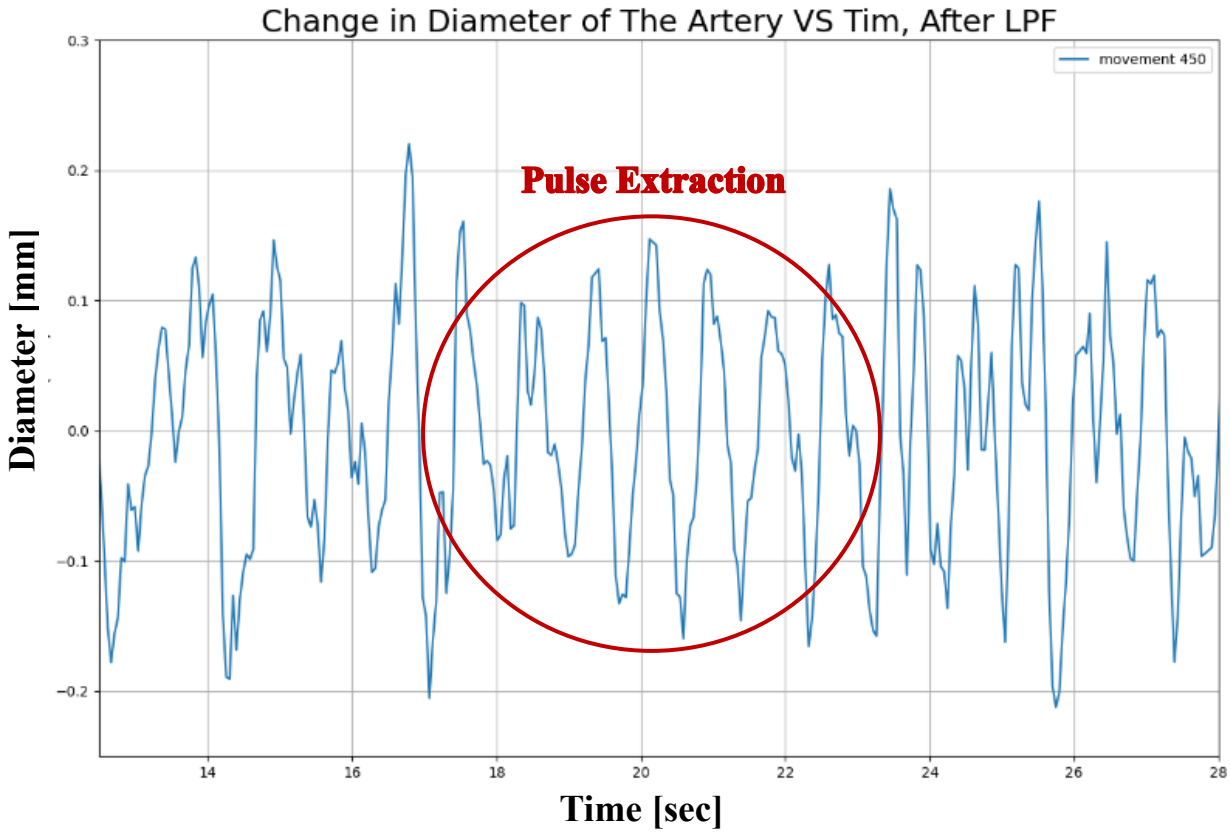

Figure 24: *Pulse Extraction Rough Estimation:*
6 pulses in 5 seconds corresponding to a 72[BPM] Heart Rate

Challenges and Solutions

Challenge: Distinguishing Arteries from Veins

A critical challenge was ensuring measurements were obtained from the radial artery (RA) rather than veins, as venous blood pressure is clinically insignificant and lacks the pulsatile characteristics necessary for accurate heart rate and blood pressure estimation.

Solution: Verification of Arterial Pulsation

To address this, we verified the presence of a distinct pulsatile signal within the region of interest (ROI) observed via the IR camera. By analyzing this signal in the RA ROI, we confirmed the structure under observation was indeed the radial artery. This verification was crucial for ensuring the reliability and validity of the extracted heart rate data and subsequent blood pressure estimations.

Challenge: Light Scattering in Tissue: Biological tissues, such as skin, cause significant scattering of IR light, making it challenging to clearly identify arterial boundaries. This scattering can blur the edges and reduce the accuracy of measurements.

Solution: Take shorter time frames and divide the video sample to smaller portions.

Hand Movement Issues: The movement of the hand during data capture creates additional variability and noise, which often causes the binary algorithm to fail in consistently identifying arterial boundaries. This can lead to inaccuracies and necessitates further algorithm refinement.

Solution: Take shorter time frames and divide the video sample to smaller portions.

Future Challenge: Arterial Volume Calculation: Changes in volume are used as a proxy for blood pressure using the established formulae from literature – we must extract several coefficients that are per patient beforehand (Appendix [A]).

Testing and Results

Out of the 10 videos analyzed, 7 yielded usable results, as summarized in Table 1. We assessed the data using two methods:

1. Identifying the main peak in the FFT analysis to determine the dominant frequency corresponding to the heart rate.
2. Extracting heart rate patterns directly from the time domain graphs, where periodic arterial diameter fluctuations were tracked.

The table below shows a comparison of heart rate measurements taken with a smartwatch, extracted from the time domain graph, and extracted from the FFT analysis:

Participant	Pulse measured with smartwatch as refernce [bpm]		Pulse extracted out of the time domain graph [bpm]		Pulse extracted out of the frequency domain graph [bpm]	
	Beginning of measurement	End of measurement			Main lobe	Secondary lobe
Amit	64	64	64 ± 2		66	
Amit (post-exercise)	120	102	105 ± 2		101.34	116.1
Amit	65	63	54.3 ± 2		57.78	
Amit	66	63	55 ± 2		73.8	61.8
Michael	72	69	68 ± 2		69	
Michael	72	72	67 ± 2		69.6	
Michael	75	75	70.5 ± 2	75 ± 2	76.56	

Table 2: Human experiments summarized heart-rate results table
*A comprehensive explanation of the experimental methodology is provided in appendix [D].

Results Analysis

We measured heart rates at rest and during exercise, noting significant variations. Smartwatch readings varied by up to 5 beats per minute (bpm) between measurements, highlighting inherent variability in wearable devices. Cuff-based monitors showed differences of about 3 bpm between pulses at the start and end of recordings, suggesting that variations up to 5 bpm are expected due to measurement uncertainties and physiological fluctuations.

During exercise, heart rate fluctuations increased dramatically, varying by 20–30 bpm within a single minute. Video data was noisy due to motion artifacts from breathing and hand movements. Despite these challenges, we validated our system by analyzing the videos in both the time domain and frequency domain using Fast Fourier Transform (FFT).

FFT analysis typically detected the primary heart rate peak, with deviations up to 10 bpm compared to reference measurements—aligning with expected variations from measurement inaccuracies and physiological changes. Time-domain analysis provided consistent results during rest but was less reliable during exercise due to increased noise.

Our system can identify heart rate patterns under controlled conditions, but accuracy decreases with significant motion artifacts or physiological variations. Deviations of less than 5 bpm in FFT analysis are considered acceptable given the experimental conditions and reference tool variability.

Performance Evaluation

The primary objective of this study was to determine whether the system could reliably measure heart rate under varying conditions. The results indicate partial success:

1. **Resting Conditions:** High accuracy was observed, with most FFT measurements aligning within 5 bpm of the reference values.
2. **Exercise Conditions:** While the system identified heart rate patterns, noise and motion artifacts reduced accuracy, leading to deviations of up to 10 bpm.
3. **Limitations of Reference Measurements:** Smartwatch readings were occasionally inconsistent, adding uncertainty to the validation process.

Further validation using a photoplethysmography (PPG) device is required to conclusively assess the system's accuracy. Unfortunately, the PPG device ordered for the study is unavailable until December, preventing its inclusion in this experiment. Future work will focus on integrating PPG data to establish ground truth measurements and improve cross-validation.

Interpretation of Findings

- Accuracy Under Resting Conditions: The system demonstrates high accuracy when subjects are at rest, with minimal discrepancies between the different measurement methods. This suggests that the system is reliable for monitoring heart rate in low-movement environments.
- Challenges During Exercise: The increased discrepancies post-exercise highlights the limitations of the system in dynamic conditions. Motion artifacts significantly impact the signal quality, reducing the reliability of both time domain and FFT analyses.
- Individual Variability: The differing levels of accuracy between participants indicate that individual physiological differences affect the system's performance. Factors such as skin properties, blood flow, and movement patterns may influence the signal detection and processing.

Possible Reasons for Discrepancies

- Motion Artifacts: During and after exercise, increased movement from breathing and muscle activity introduces significant noise, affecting the accuracy of both time domain and FFT analyses.
- Physiological Fluctuations: Heart rate can change rapidly during recovery from exercise, leading to transient variations that may not be captured accurately in short recording intervals.
- Signal Overlap and Noise: The FFT may detect multiple frequency components, especially in noisy signals, resulting in multiple peaks that complicate the identification of the true heart rate.
- Smartwatch Limitations: Consumer-grade smartwatches may have their own measurement inaccuracies, particularly during high-intensity activities when sensor contact can be less stable.

Recommendations for Improvement

- Motion Artifact Reduction: Implement advanced filtering techniques, such as adaptive filters or independent component analysis, to mitigate the impact of motion artifacts on the signal.
- Improved Reference Standards: Utilize medical-grade heart rate monitors or ECG/PPG devices for more accurate reference measurements, reducing the uncertainty associated with smartwatch data.
- Participant Instructions: Provide clear instructions to participants to minimize movement during recordings, even after exercising, to enhance signal quality. Use fixating device to stabilize the subject's wrist.

Future Work

To enhance the system's accuracy and broaden its applicability, future research will focus on several key areas:

1. Blood Pressure Estimation: Using established physiological formulas (Appendix [A]), subject-specific constants and coefficients will be calculated to extract BP values from heart rate data, further expanding the system’s functionality and achieving one the project's main goals.
2. Integration of Photoplethysmography (PPG) Data: The acquisition of a PPG device will allow for more precise ground truth measurements. Incorporating PPG data will enable more rigorous validation of the system's performance and help in fine-tuning the algorithms used for heart rate detection.
3. Expansion of the Participant Pool: Increasing the number of participants and including a more diverse demographic and subjects with different skin tones will help in assessing the generalizability of the system. This expansion can provide insights into how different physiological characteristics affect the system's performance.

4. Comparative Studies with Established Methods: Conducting comparative analyses with established heart-rate monitoring and BP extraction methods will provide a clearer understanding of the system's advantages and limitations. This comparison can guide further improvements and identify specific use cases where the system excels.

Project's Conclusions and Insights

Discussion

The findings from our study indicate that the proposed system has the capability to detect heart rate patterns under controlled, resting conditions with a reasonable degree of accuracy. The time domain analysis provided results that were consistent with the reference measurements obtained from the smartwatch, particularly when the subjects were at rest and motion artifacts were minimal. The FFT analysis further supported these findings by identifying dominant frequency peaks that corresponded closely to the heart rates measured by the smartwatch.

However, the system's accuracy diminished during exercise conditions. The increased motion artifacts resulting from breathing and hand movements introduced significant noise into the video data, making it challenging to extract reliable heart rate signals. This limitation highlights the difficulty of non-invasive heart rate monitoring using video analysis in dynamic environments where motion is prevalent.

It is also important to acknowledge that the majority of BP measurements are conducted under resting conditions using conventional methods such as sphygmomanometers (BP cuffs). This highlights the practical relevance of optimizing the system for resting-state monitoring, aligning it with standard clinical and ambulatory care practices.

Conclusion

Our findings demonstrate the potential of our novel method for blood pressure (BP) measurement. Continued development is essential to enhance accuracy, extract reliable BP values, and validate the approach through comparisons with conventional methods such as BP cuffs. During this project we developed a pioneering non-invasive approach that employs optical imaging and advanced image processing algorithms to estimate heart rate and, in the future, extract blood pressure with improved accuracy and reliability.

This project serves as a foundation for non-invasive blood pressure monitoring technologies, offering insights and methodologies that can be refined and expanded upon in future research endeavors. It exemplifies the intersection of engineering, physics, and healthcare, demonstrating the potential of technology to revolutionize medical diagnostics.

References

1. Wang, C., et al., "Monitoring of the Central Blood Pressure Waveform via a Conformal Ultrasonic Device", Nature Biomedical Engineering, 2018. https://www.ncbi.nlm.nih.gov/pmc/articles/PMC6428206/

2. Pallarés-Carratalá, V., Ruiz-García, A., Serrano-Cumplido, A., Arranz-Martínez, E., Divisón-Garrote, J. A., Moyá-Amengual, A., Escobar-Cervantes, C., & Barrios, V. (2023). Prevalence Rates of Arterial Hypertension According to the Threshold Criteria of 140/90 or 130/80 mmHg and Associated Cardiometabolic and Renal Factors: SIMETAP-HTN Study. *Medicina*, *59*(10), 1846. https://doi.org/10.3390/medicina59101846

3. Muhammed, S. (2022). Radial Artery. *Mickey Med*. Retrieved from https://www.mickeymed.com/article/radial_artery

4. Cleveland Clinic. (n.d.). High Blood Pressure (Hypertension). Retrieved from https://my.clevelandclinic.org/health/diseases/4314-hypertension-high-blood-pressure

5. Garcia, J., Rios, P., Rivera, N., Diaz, M., & Rivas, E. (2021). Competitive Real-Time Near Infrared (NIR) Vein Finder Imaging Device to Improve Peripheral Subcutaneous Vein Selection in Venipuncture for Clinical Laboratory Testing. *ResearchGate*. Retrieved from https://www.researchgate.net/publication/350519039_Competitive_Real-Time_Near_Infrared_NIR_Vein_Finder_Imaging_Device_to_Improve_Peripheral_Subcutaneous_Vein_Selection_in_Venipuncture_for_Clinical_Laboratory_Testing

6. "BioBeat's Cuffless Blood Pressure Monitoring Device, USA." *Medical Device Network*. https://www.medicaldevice-network.com/projects/biobeats-cuffless-blood-pressure-monitoring-device-usa/

7. "Near-infrared window in biological tissue." *Wikipedia*, https://en.m.wikipedia.org/wiki/Near-infrared_window_in_biological_tissue

8. ZWO Optical. (n.d.). ASI990MM-PRO & ASI991MM-PRO Cameras. Retrieved from https://www.zwoastro.com/product/asi990mm-pro-asi991mm-pro/

9. Bosschaart, N., Edelman, G. J., Aalders, M. C. G., van Leeuwen, T. G., & Faber, D. J. (2014). A literature review and novel theoretical approach on the optical properties of whole blood. *Lasers in Medical Science*, *29*(2), 453–479. https://doi.org/10.1007/s10103-013-1446-7

10. Kim, S., Lim, Y. T., Soltesz, E. G., De Grand, A. M., Lee, J., Nakayama, A., Parker, J. A., Mihaljevic, T., Laurence, R. G., Dor, D. M., Cohn, L. H., Bawendi, M. G., & Frangioni, J. V. (2010). Near-infrared fluorescent type II quantum dots for sentinel lymph node mapping. *Nature Nanotechnology*, *5*(6), 465–469. https://doi.org/10.1038/nnano.2009.326

Appendices

Appendix [A] – The arterial BP waveform $p(t)$ appears as follows:

$$(\mathbf{1})\ \textbf{Artery Diastolic Pressure}:\quad p(t) = p_d \times e^{\alpha\left[\frac{A(t)}{A_d}-1\right]}$$

- $A_d - Diastolic\ Arterial\ Cross - Section\ Coeffcient$
- $p_d - Diastolic\ Pressure\ Coefficient$
- $d(t) - Diameter\ Waveform\ of\ Target\ Artery$
- $\alpha - Vessel\ Rigidity\ Coefficient$

Assuming that artery is rotationally symmetrical, $A(t)$ can be calculated as: where p_d is diastolic pressure,
A_d is the diastolic arterial cross-section and α is the rigidity

$$(\mathbf{2})\ \boldsymbol{Artery\ Volume\ Change}\ (\boldsymbol{Area}):\ A(t) = \frac{\pi d^2(t)}{4}$$

where $d(t)$ is the diameter waveform of the target artery.
α can be calculated by equation:

$$(\mathbf{3})\ \boldsymbol{\alpha} = \frac{\boldsymbol{A_d \ln\left(\frac{p_s}{p_d}\right)}}{\boldsymbol{A_s - A_d}}$$

for α and p_d, the accurate pressure waveform $p(t)$ can be achieved. Measured by commercial BP cuff. Using the aforementioned equation and a brief calibration where in A_s is the systolic arterial cross-section, p_s is the systolic pressure which can be coefficient.

Appendix [B] – LEDs with various wavelengths used in the experiments:

- **M1550L4 (1550 nm)**: Deep tissue penetration, but with significant water absorption, suitable for large tissue depths.
- **M1450L4 (1450 nm)**: Sensitive to water absorption; used for detecting superficial tissue layers.
- **M1050L4 (1050 nm)**: Offers good balance between penetration and scattering, ideal for capturing arterial changes.
- **M970L4 (970 nm) & M940L3 (940 nm)**: Medium penetration depth, useful for near-surface tissue analysis.
- **850nm LED**: High tissue penetration, frequently used in medical imaging.
- **680nm LED**: Less tissue penetration, ideal for detecting surface-level changes.

Appendix [C] – frequency domain changes in the diameter of the RA VS Frequency:

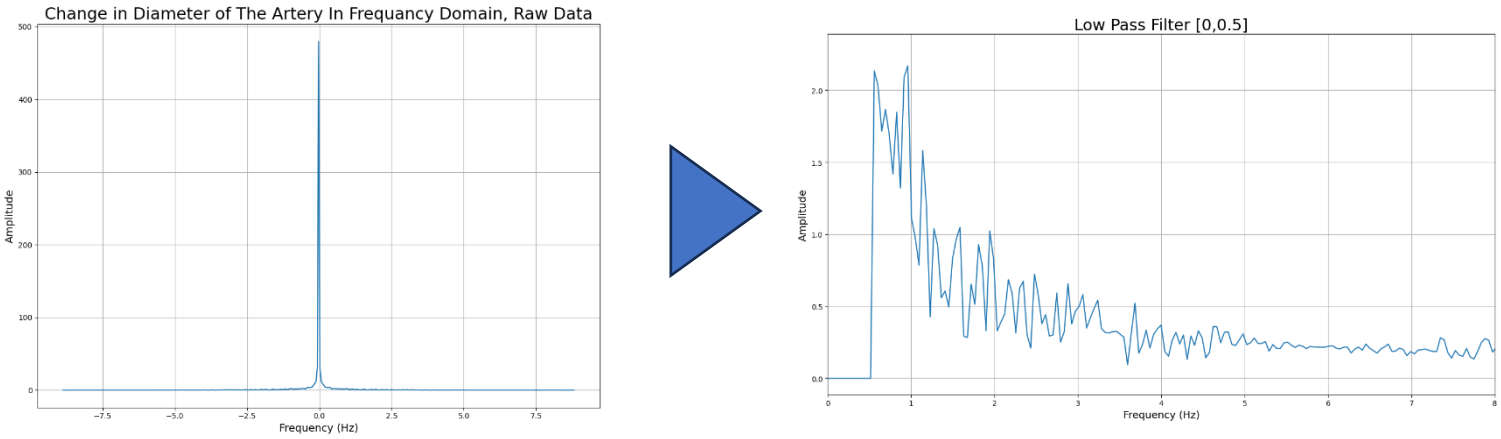

Figure 27: Raw Data frequency domain changes in the diameter [mm] of the RA VS Frequency [Hz]
Left: FFT of raw measurement of dimeter of the RA in time
Right: Positive frequency of FFT after applying LPF

Appendix [D] – Raw Image – metal object on skin for different wavelengths comparison:

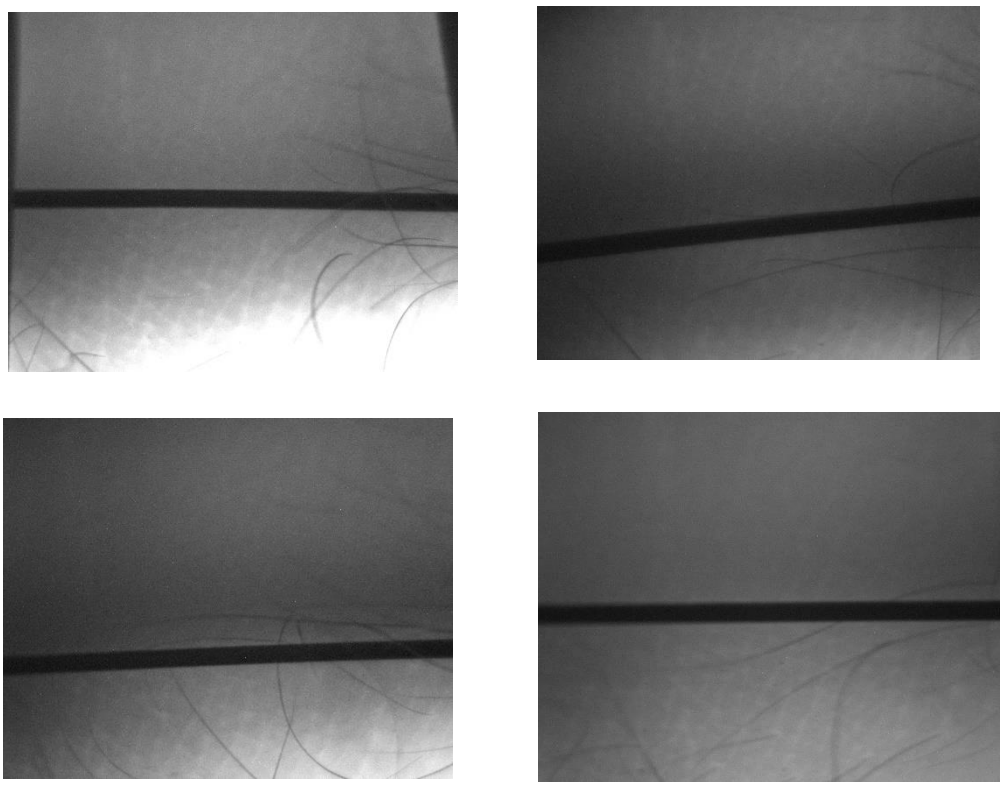

Figure 27: Different Wavelength with metal object comparison
1) Top-Left: 850nm **2) Top-Right:** 940nm 3**) Bottom-Left:** 970nm **4) Bottom-Right:** 1050nm

Appendix [E] – Results full analysis graphs:

Amit pulse measured via smart watch measurement:
beginning the video measurement: 64 bpm
at the end of the video measurement: 64 bpm

FFT result:
main lobe: 66.3 bpm

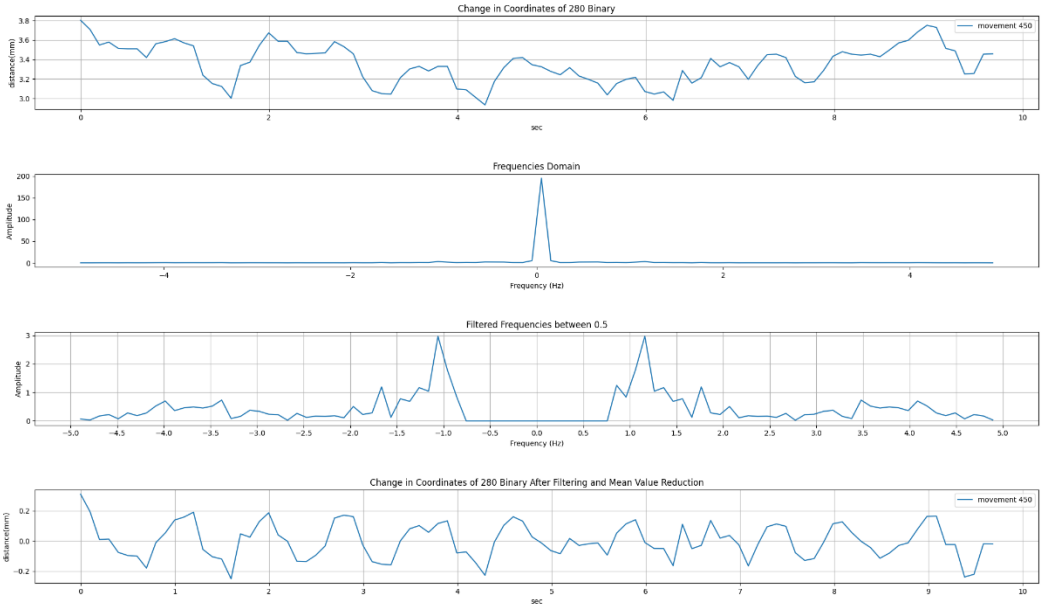

In time domain:
We measured pulse of 65.4 bpm [in 5.5 seconds we identify 6 pulses]

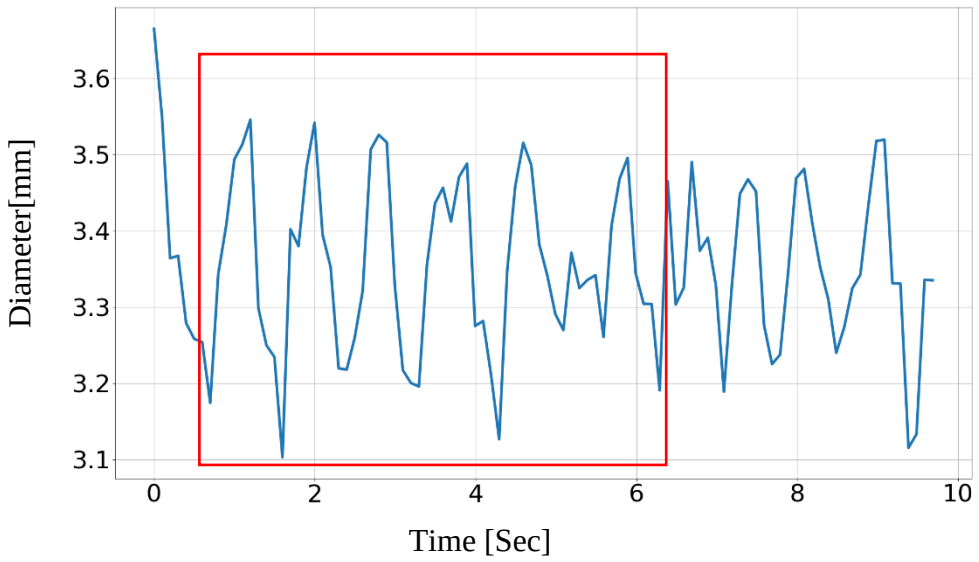

Amit pulse measured via smart watch measurement:
beginning the video measurement: 102 bpm
at the end of the video measurement: 120 bpm

FFT result:
main lobe: 101.34 bpm
Secondary lobe: 116.1

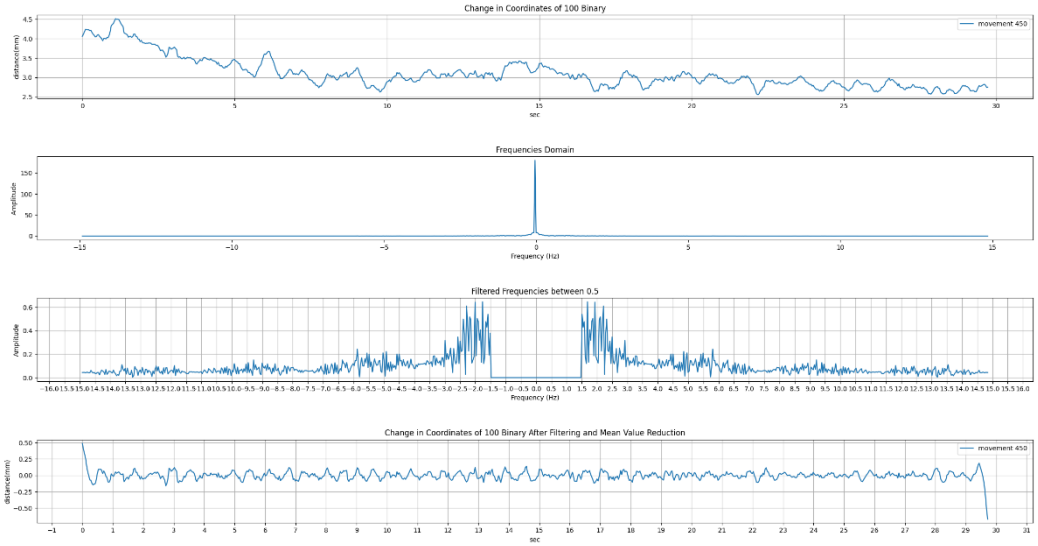

In time domain:
We measured pulse of 105.8 bpm [in 5.1 seconds we identify 9 pulses]

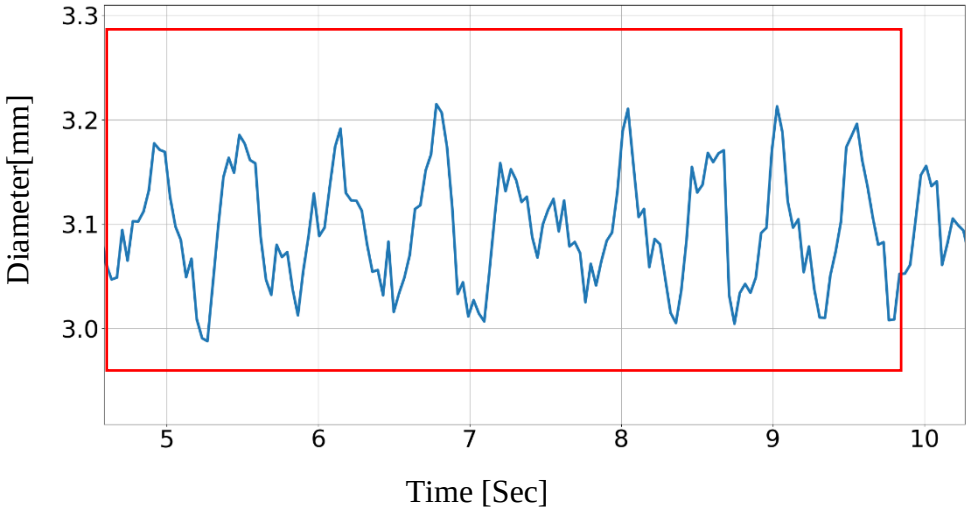

Misha pulse measured via cuff blood measurement:
beginning the video measurement: 72 bpm
at the end of the video measurement: 68 bpm

FFT result:
main lobe: 69 bpm

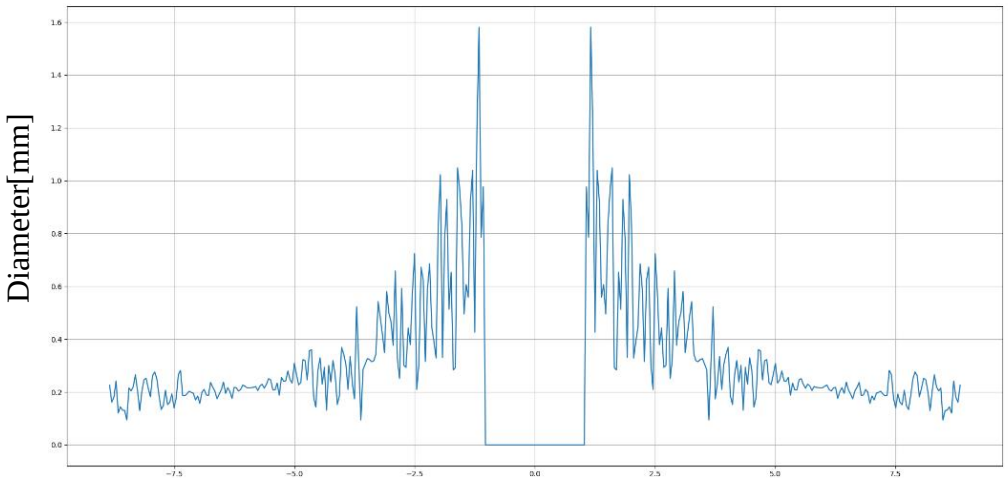

In time domain:
we measured pulse of 68 bpm [in 10 seconds we identify 12 pulses]

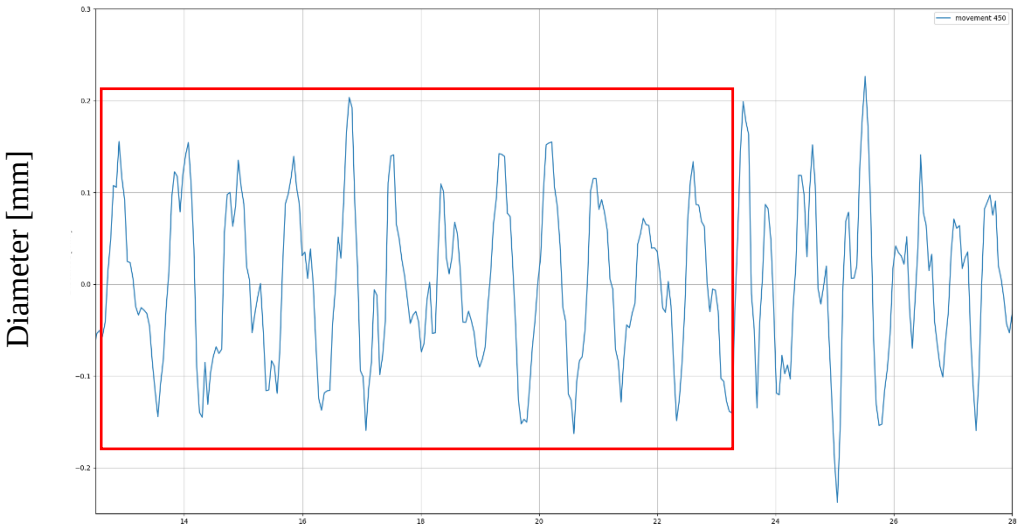

Misha pulse measured via cuff blood measurement:
beginning the video measurement: 72 bpm
at the end of the video measurement: 72 bpm

FFT result:
main lobe: 69.6 bpm

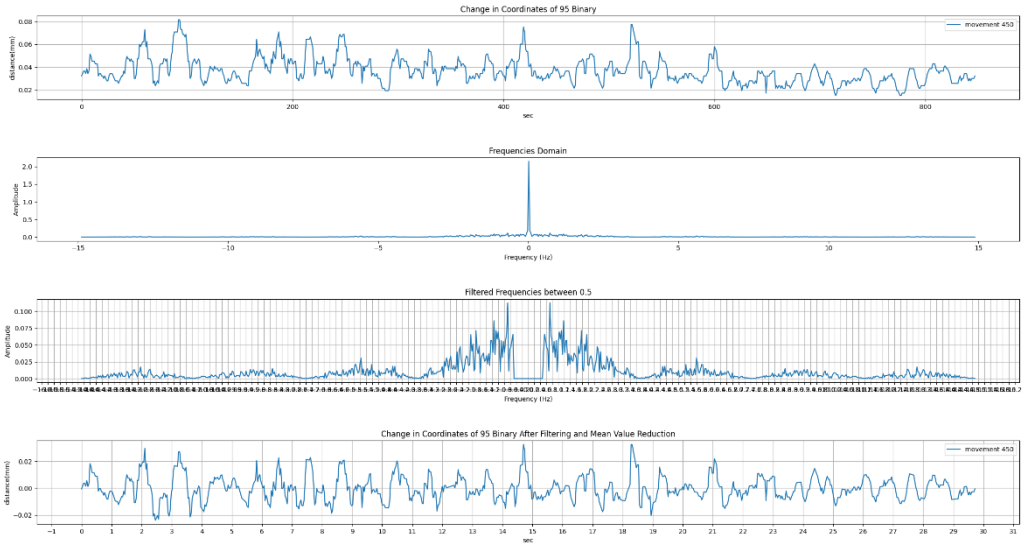

In time domain:
We measured pulse of 67 bpm [in 5.3 seconds we identify 6 pulses]

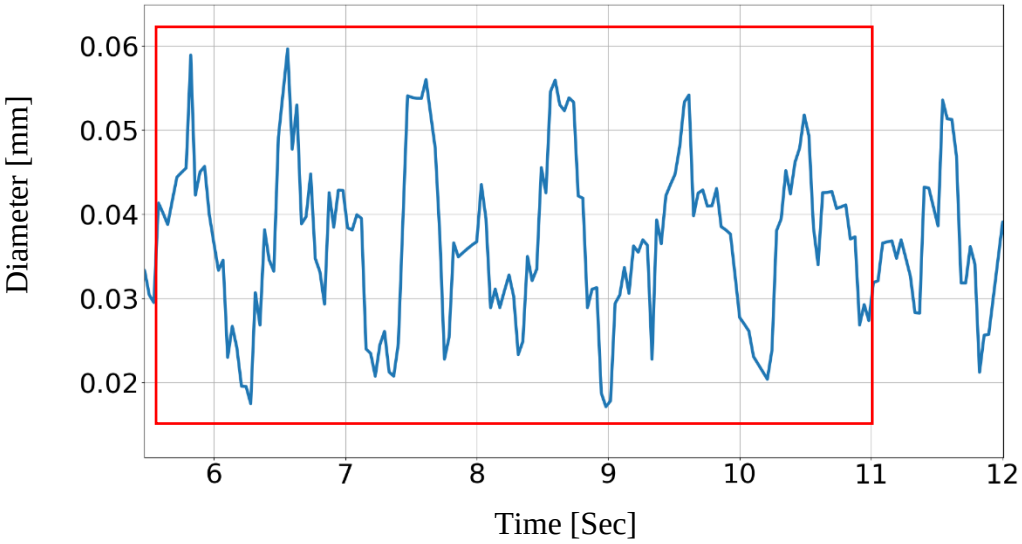

Amit pulse measured via cuff blood measurement:
beginning the video measurement: 63 bpm
at the end of the video measurement: 65 bpm

FFT result:
main lobe: 74.16 bpm
secondary lobe: 83.76 bpm
third lobe: 64.56 bpm
*The second and the third lob have almost same amplitude in the frequency domain

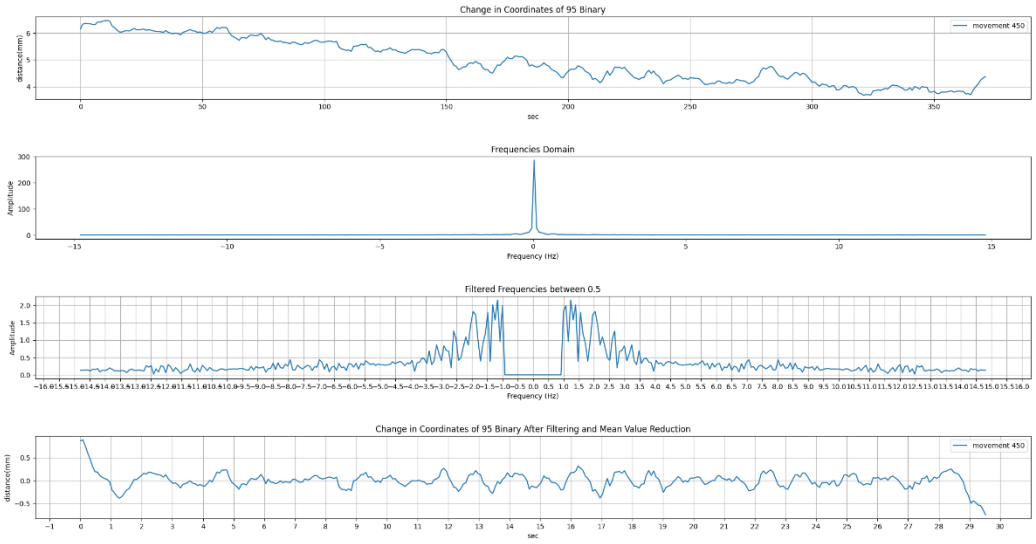

In time domain:
we measured pulse of 54.3 bpm [in 7.73 seconds we identify 7 pulses]

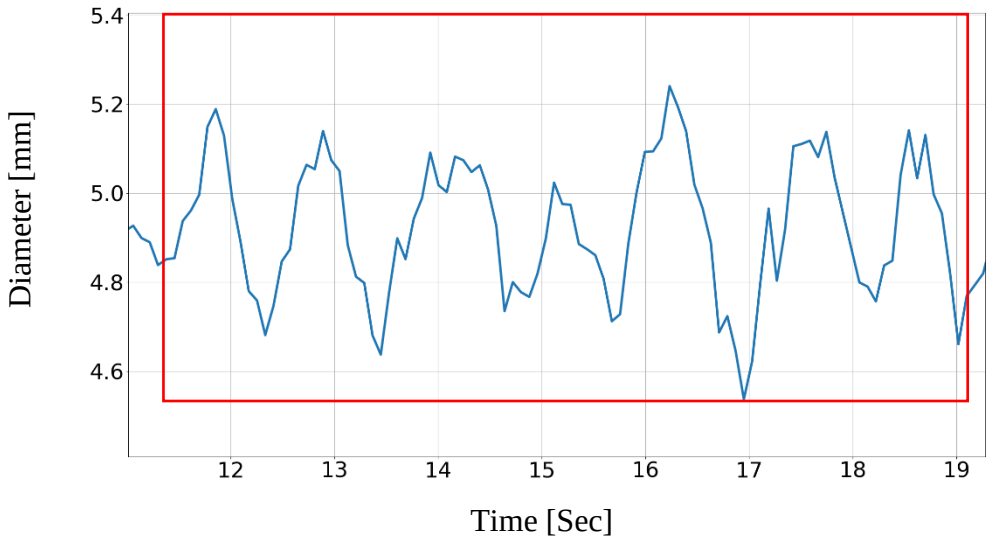

Amit pulse measured via cuff blood measurement:
beginning the video measurement: 63 bpm
at the end of the video measurement: 66 bpm

FFT result:
main lobe: 73.8 bpm
secondary lobe: 61.8 bpm

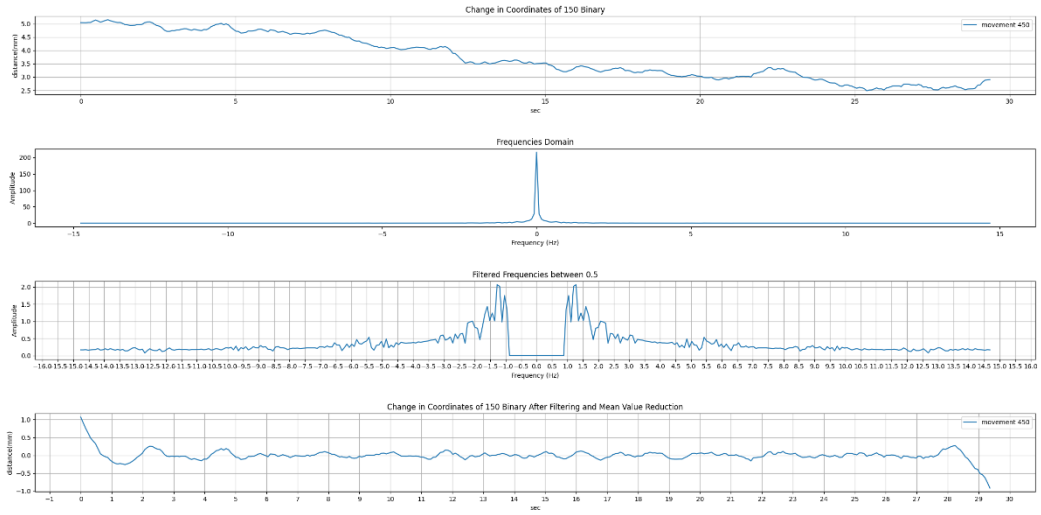

In time domain:
we measured pulse of 55.5 bpm [in 5.4 seconds we identify 5 pulses]

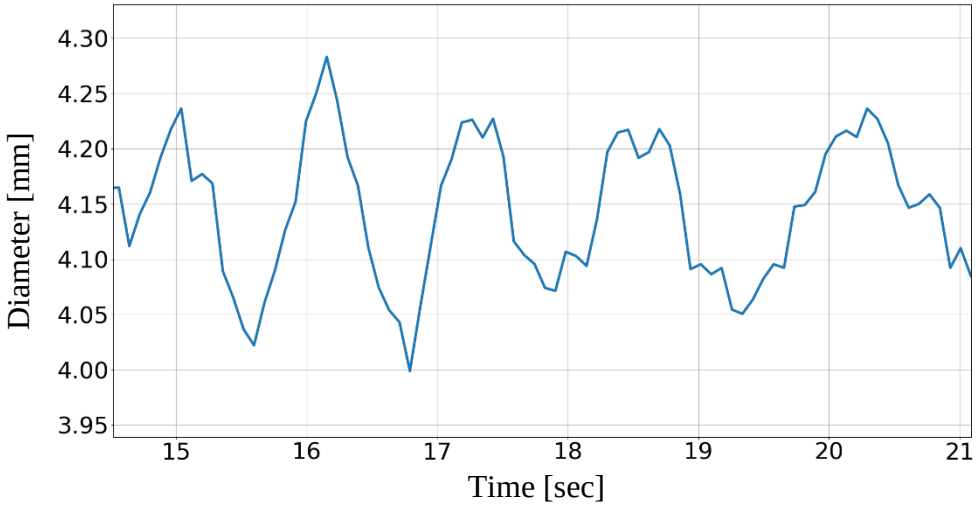

Amit pulse measured via cuff blood measurement:
beginning the video measurement: 75 bpm
at the end of the video measurement: 75 bpm

FFT result:
main lobe: 76.56 bp

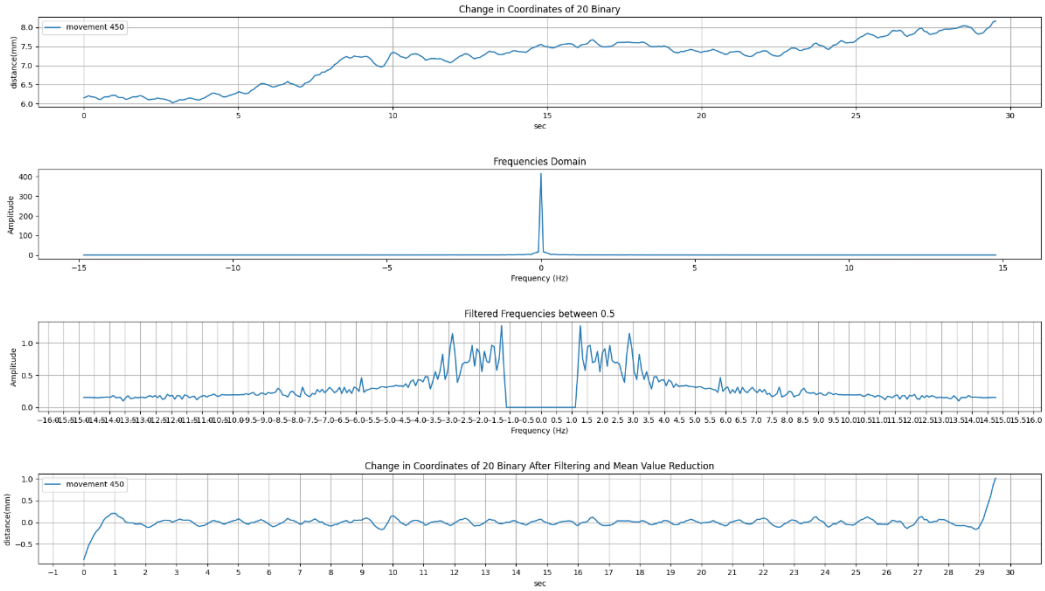

In time domain:
we measured pulse of 71.4 bpm [in 4.2 seconds we identify 5 pulses]
and in the second are we measured pulse 75 bpm [in 7.2 seconds we identify 9 pulses]